pp60^{src} Tyrosine Kinase Modulates P19 Embryonal Carcinoma Cell Fate by Inhibiting Neuronal but Not Epithelial Differentiation

John W. Schmidt,*‡ Joan S. Brugge,‡ and W. James Nelson*

*Department of Molecular and Cellular Physiology, Stanford University School of Medicine, Stanford, California 94305-5426; and ‡Department of Microbiology and Howard Hughes Medical Institute, University of Pennsylvania School of Medicine, Philadelphia, Pennsylvania 19104-6148

Abstract. P19 embryonal carcinoma cells provide an in vitro model system to analyze the events involved in neural differentiation. These multipotential stem cells can be induced by retinoic acid (RA) to differentiate into neural cells. We have investigated the ability of several variant forms of the protein-tyrosine kinase (PTK) pp60^{src} to modulate cell fate determination in this system. Normally, P19 cells are induced to differentiate along a neural lineage when allowed to form extensive cell–cell contacts in large multicellular aggregates during exposure to RA. Through analysis of markers of epithelial (keratin and desmosomal proteins) and neuronal (neurofilament) cells we have found that RA-induced P19 cells transiently express epithelial markers before neuronal differentiation. Under these inductive conditions, expression of pp60$^{v\text{-}src}$ or expression of the neuronal variant pp60$^{c\text{-}src+}$ inhibited neuronal differentiation, and resulted in maintained expression of an epithelial phenotype. Morphological analysis showed that expression of pp60^{src} PTKs results in decreased cell–cell adhesion during the critical cell aggregation stage of the neural differentiation procedure. The effects of pp60$^{v\text{-}src}$ on cell fate and cell–cell adhesion could be mimicked by direct modulation of Ca^{++}-dependent cell–cell contact during RA induction of normal P19 cells. We conclude that the neural lineage of P19 cells includes an early epithelial intermediate and suggest that tyrosine phosphorylation can modulate cell fate determination during an early cell–cell adhesion-dependent event in neurogenesis.

CELL-cell signals are important regulators of cell fate (45) and receptors that couple to protein-tyrosine kinases (PTKs)[1] are one class of mediators of these signals (56). PTKs have been implicated in events regulating neuronal differentiation and survival (4, 29). We have investigated the effect of pp60^{src} PTKs on a neuronal cell fate decision in an in vitro model system. In most cells the c-*src* gene codes for a 60 kD phosphoprotein which has protein-tyrosine kinase activity (termed pp60$^{c\text{-}src}$). However, neurons from the central nervous system express a variant form of pp60$^{c\text{-}src}$ (8) that contains a six-amino acid insert due to alternate splicing of the c-*src* mRNA which codes for pp60$^{c\text{-}src+}$ (38, 43). The v-*src* gene codes for the transforming protein of Rous sarcoma virus, pp60$^{v\text{-}src}$. The pp60$^{v\text{-}src}$ protein is a mutant variant of pp60$^{c\text{-}src}$ that is constitutively activated, escaping the negative regulation of pp60$^{c\text{-}src}$ that normally occurs in cells (11, 25).

The murine P19 embryonal carcinoma cell line (44) offers an in vitro system for investigating mechanisms of neurogenesis and the roles of candidate regulatory proteins such as pp60$^{c\text{-}src}$. P19 cells have characteristics of a multipotential stem cell. When P19 cells are introduced into mouse embryos they participate in the development of most tissues (58). P19 cells can be induced to differentiate into neurons in vitro by a combination of exposure to retinoic acid (RA) and cell aggregation (28). Undifferentiated P19 cells have a low level of pp60$^{c\text{-}src}$, whereas these cells express a high level of the neuronal variant pp60$^{c\text{-}src+}$ after neural differentiation (41). Retroviral transduction of the v-*src* gene has previously been used to immortalize committed neural cells isolated from developing animals (10). In P19 cells, v-*src* has been shown to block neurogenesis (5). However, in primary sympathetic neurons (23) and PC12 cells (2) pp60$^{v\text{-}src}$ promotes neuronal differentiation. These apparently contradictory observations may be reconciled if tyrosine phosphorylation has different effects at different points in the neural lineage.

Neural differentiation of P19 cells is promoted by the establishment of extensive cell–cell contact when cells are grown as aggregates during exposure to RA (44). In contrast, P19 cells exposed to RA in the absence of extensive cell-cell contact differentiate into cells with a flattened morphology, some of which have detectable keratin intermediate filaments (48). The molecules involved in the cell–cell contact of differentiating P19 cells in vitro have not been extensively analyzed. A predominant calcium-dependent cell–cell

1. *Abbreviations used in this paper*: DP, desmoplakin; NF-M, middle molecular weight neurofilament protein; PTK, protein-tyrosine kinase; RA, retinoic acid.

adhesion molecule of the early mouse embryo (66) and P19 cells (49) is E-cadherin. E-cadherin expression is lost when most cell types differentiate, but many epithelial cells retain E-cadherin (66). E-cadherin-mediated adhesion is thought to be at the beginning of a cascade of cell adhesion-dependent events in the establishment of extensive cell-cell contacts and epithelial polarity (57). Neural commitment occurs in the embryonic ectoderm and neural differentiation continues in neuroepithelia. Results concerning the role of cadherins in other epithelia may be relevant to neural induction in ectoderm in vitro and P19 cells in vitro. In MDCK epithelial cells, pp60$^{v\text{-}src}$ disrupts cell-cell adhesion at the intercellular junctional complex where E-cadherin is localized (69). Similarly, in lens epithelial cells, pp60$^{v\text{-}src}$ causes deterioration of N-cadherin-rich adherens junctions (68). These alterations in cell-cell contact due to pp60$^{v\text{-}src}$ in epithelial cells suggest that pp60$^{v\text{-}src}$ might also decrease cell-cell adhesion of P19 cells.

We have investigated the effect of over-expression of pp60$^{c\text{-}src}$ and further investigated the effects of pp60$^{v\text{-}src}$ on the neural differentiation of P19 cells. During the course of these investigations we found that stock (parental) P19 cells transiently express an epithelial phenotype during RA-treatment of cell aggregates, before expression of a neuronal phenotype. Both pp60$^{v\text{-}src}$- and pp60$^{c\text{-}src+}$-expressing P19 cells retain the capacity for RA-induced epithelial differentiation, but they have a reduced capacity for neuronal differentiation. The pp60$^{v\text{-}src}$- and pp60$^{c\text{-}src+}$-expressing P19 cells also display reduced cell-cell adhesion in RA-treated aggregates. Reduction of cell-cell adhesion and inhibition of neurogenesis in RA-treated stock cell aggregates could also be achieved by culturing the aggregates in medium with a low concentration of calcium. These results raise the possibility that the pp60^{src}-mediated block of neuronal differentiation may be due, at least in part, to pp60^{src}-mediated reduction in cell-cell adhesion.

Materials and Methods

Primary Antibodies

The Endo-A keratin-reactive TROMA-1 mouse monoclonal IgG (30) was hybridoma culture supernatant obtained from Rolf Kemler, Max-Planck, Tubingen. The anti-E-cadherin rabbit antiserum was also obtained from Rolf Kemler. This antiserum was produced using mouse E-cadherin as antigen as described previously (67). The rabbit antidesmoplakin antiserum was prepared as previously described (55). The anti-pp60^{src} mouse monoclonal IgG 327 (39) was purified from ascites fluid. 327 reacts with mouse and chicken pp60^{src}. The chicken specific anti-pp60^{src} mouse monoclonal IgG EC10 (54) was from hybridoma culture supernatants. The stem cell-reactive anti-SSEA-1 mouse monoclonal IgM (62) was an ascites fluid obtained from Barbara Knowles, Wistar Institute. The antineurofilament mouse monoclonal IgG was RMO308 (33) hybridoma culture supernatant obtained from Virginia Lee, University of Pennsylvania. The anti-phosphotyrosine-reactive mouse monoclonal IgG was purified PY20 (19) obtained from ICN Biomedicals (Costa Mesa, CA). Antiglial fibrilary acidic protein rabbit antiserum was from DAKO Corp. (Carpinteria, CA). Antidesmin mouse mAb was from Labsystems (Helsinki, Finland). The antivimentin rabbit antiserum was previously described (51).

Plasmids and Viruses

For expression plasmids chicken c-*src* (37), c-*src*$^+$ (38), or Schmidt-Rupin A strain of RSV v-*src* sequences (13) were used allowing easy detection of plasmid expressed pp60^{src} using mAb EC10. Plasmids pLNSL7v-*src*, pLNCXc-*src*$^+$, and pLNCXc-*src* were constructed by ligation of *src* into the ClaI sites of pLNCX and pLNSL7 (46). Psi-2 cells were transfected using the calcium phosphate precipitation technique (12) with the retroviral packaging signal containing plasmids. Each plasmid has the *neo* gene under the control of the retroviral long terminal repeat. Transfected clonal lines were selected by growth of cells in G418. Viral culture supernatants were stored at −80°C and viral titers assayed on NIH3T3 cells. Viral supernatants from Psi-2 lines which had good titer and gave expression of pp60^{src} in 3T3 cells were used for infection of stock undifferentiated P19 cells. Infections were performed by adding viral supernatants to cell cultures in the presence of 8 μg/ml polybrene.

Cells

The P19 cells were mouse P19S18O1A1 cells obtained from Joel Levine, SUNY, Stony Brook. P19 cells were cultured in high glucose DMEM as described previously (35) except for experiments involving immunohistochemical detection of Endo-A keratin expression for which DMEM/F12 and gelatin-coated coverslips were used as described (48). The cells grew more slowly under the later conditions, and keratin filaments were easier to visualize by staining. Exposure of monolayer cultures to retinoic acid was as described (48). F9 cells were grown under the same conditions as P19 cells. RA was included in culture media at one feeding and the cells were refed after 2 d with normal medium. Neuronal differentiation was achieved by RA treatment of cells allowed to aggregate in bacteriological grade culture dishes according to the protocol of Levine and Flynn (35) except that poly-D-lysine was used during growth in serum-free medium. For growth of cells in low calcium medium and metabolic labeling experiments, dialyzed FCS was used. Mouse NIH3T3 (ATCC) and Psi-2 (42) cells were maintained in high glucose DMEM with 10% calf serum. G418-resistant cells were selected in 400 μg/ml G418 and maintained in 200 μg/ml G418 until the last feeding before viral supernatant collection (Psi-2 cells) or 2 d before RA treatment for P19 cells. Initial experiments involving neuronal differentiation were performed with four sublines each of pp60$^{c\text{-}src+}$- and pp60$^{v\text{-}src}$-expressing P19 cells. For further analysis (see Figs. 5, 7 *C*, *F*, and *G*, 8, *E–G*, and most E-cadherin experiments) two sublines designated CXcsrc$^+$E7 and SLvsrc3E were used. These lines were shown to have stable expression of pp60^{src} from their retrovirally introduced *src* genes in the absence of continued G418 selection. MDCK cells were maintained as described previously (51).

Phosphorylation

In vitro protein-tyrosine kinase (PTK) assays were performed following immunoprecipitation of pp60^{src} as described (8) except that Mn^{++} was used instead of Mg^{++} in some experiments and protein A-Sepharose was used instead of *S. aureus* cells. For quantitation of in vitro PTK activity Mg^{++} was used, the reaction was for 10 min at 4°C, and ^{32}P incorporated into enolase was directly measured in excised gel slices. RIPA buffer (1% deoxycholate, 1% TX-100, and 0.1% SDS, 160 mM NaCl, 5 mM EDTA, and 10 mM Tris, pH 7.2) was used to solubilize pp60^{src}.

Quantitative Determination of Protein Levels

Transfer of proteins to nitrocellulose and detection of specific proteins with antibodies and ^{125}I-protein A was performed as described previously (55), except that transfer currents were varied from 0.5 to 0.75 Amp·h depending on the M_r of the protein to be detected. For desmoplakin experiments protein solubilization conditions with nonionic detergent (CSK, contains 0.5% TX-100) and SDS were as described (55). For detection of phosphotyrosine-containing proteins, cells were removed from culture dishes by scraping in hot SDS buffer (containing 2% SDS) as described (20). For anti-pp60^{src} and antiintermediate filament protein blots, cell pellets were frozen at −80°C and then were solubilized in SDS buffer. For keratin experiments, leupeptin was included to inhibit proteolysis. Solubilized protein was determined using the Bio-Rad protein assay (Bio-Rad Laboratories, Richmond, CA) and equal amounts of protein were electrophoresed for each sample. For blots probed with mouse mAbs, an incubation with purified rabbit-antimouse antibodies (Boehringer Mannheim Biochemicals, Indianapolis, IN) was done after the primary antibody incubation. For quantitation, pieces of nitrocellulose were cut from blots and ^{125}I counted directly or autoradiograms were scanned with a densitometer. For estimation of protein M_r according to migration distance during SDS-PAGE, prestained protein standards (Bio-Rad Laboratories) were used: myosin (213 kD), β-galactosidase (122 kD), BSA (80 kD), and ovalbumin (50 kD). For quantitation of cell surface E-cadherin, cells were washed with PBS with 1 mM Ca^{++} and

incubated for 8 min at 37°C in the same buffer with 600 μg/ml trypsin (Worthington Biochemical Corp., Freehold, NJ). PMSF and soybean trypsin inhibitor were added, cells were sedimented, and anti-E-cadherin antiserum-reactive protein was immunoprecipitated from the cell supernatants. Immunoprecipitated proteins were resolved by SDS-PAGE and transferred to nitrocellulose. Cell surface E-cadherin was detected by probing the nitrocellulose with the same anti-E-cadherin antiserum. The 84–97-kD proteolytic fragments are derived from the extracellular domain of E-cadherin.

Immunofluorescence

For SSEA-1 detection, cells were not fixed before staining. For SSEA-1 visualization, a purified goat antimouse antibody that reacts with IgM obtained from Boehringer Mannheim was used. This antibody is biotin conjugated and was visualized with Avidin-FITC from Boehringer Mannheim. For middle molecular weight neurofilament protein (NF-M), glial fibrilary acidic protein, keratin, and vimentin intermediate filament staining, cells were fixed with acetic acid/ethanol (5:95%). Mouse IgGs were visualized with a purified goat antimouse lissamine rhodamine conjugated antibody from Boehringer Mannheim. E-cadherin and desmoplakin staining was with methanol-fixed cells. Primary rabbit antibodies were visualized with rhodamine-conjugated affinity-purified goat antirabbit F(ab) from Accurate Chemical (Westbury, NY) or FITC-conjugated affinity-purified swine anti-rabbit IgG from DAKO. For aggregate staining, aggregates were embedded in gelatin and sectioned (10 μm) before staining. All cell staining was done with cells grown on poly-D-lysine–coated glass coverslips except for Endo-A keratin staining which was done with cells on gelatin coated coverslips.

Results

Expression of pp60$^{v\text{-}src}$5 or pp60$^{c\text{-}src}$ in P19 Cells

To examine the effects of expression of pp60$^{v\text{-}src}$ and overexpression of pp60$^{c\text{-}src}$ in P19 cells, sublines were generated after infection of undifferentiated cells with recombinant murine retroviruses carrying the avian v-*src* and c-*src* genes. An MLV-derived retroviral vector carrying an internal cytomegalovirus early gene promoter (LNCXc-*src*$^+$) was used for expression of pp60$^{c\text{-}src+}$ (46), and a similar vector with an internal SV40 early promoter (LNSL7v-*src*) was used to generate P19 sublines that express pp60$^{v\text{-}src}$. Expression of pp60^{src} by P19 cells was quantitated using an in vitro PTK assay following immunoprecipitation of pp60^{src} from infected P19 cells (Fig. 1 *A*, lanes *3–8* and *B*, lanes *3–5*). Based on ^{32}P incorporation into the exogenous substrate enolase, the pp60^{src} kinase activities of two LNCXc-*src*$^+$-infected and two LNSL7v-*src*–infected P19 sublines were 10.5-, 6.6-, 36-, and 43-fold higher than that of stock (noninfected) undifferentiated P19 cells (Fig. 1 *C*, lanes *1–5*).

The relative levels of pp60^{src} in two P19 sublines were also quantitated using an immunoblot assay (Fig. 2 *A*). The amount of pp60^{src} in cells of subline CXcsrc$^+$E7 (lane *2*) is eightfold higher than that of endogenous pp60^{src} in undifferentiated stock P19 cells (lane *1*). A similar level of pp60$^{c\text{-}src+}$ is expressed after neuronal differentiation of stock P19 cells (41). The level of pp60^{src} in subline SLvsrc3E (lane *3*) is fivefold higher than that of stock P19 cells. The high in vitro PTK activity of pp60^{src} from pp60$^{v\text{-}src}$-expressing P19 cells (Fig. 1 *C*) is due to the high specific activity of pp60$^{v\text{-}src}$ (11, 25). NIH3T3 cells infected with the same retroviruses displayed significantly higher levels of expression of these pp60$^{c\text{-}src}$ variants (Fig. 1 *A*, lane *1*; *B*, lane *6*; and *C*, lanes *7* and *8*), suggesting that both the CMV and SV40 early promoters are less effective in promoting transcription in P19 cells, as expected from results with other embryonal cells (21). The CMV promoter gives the best expression of pp60^{src} in P19 cells and allows investigation of the effect of a moderately elevated level of pp60$^{c\text{-}src}$ on neurogenesis.

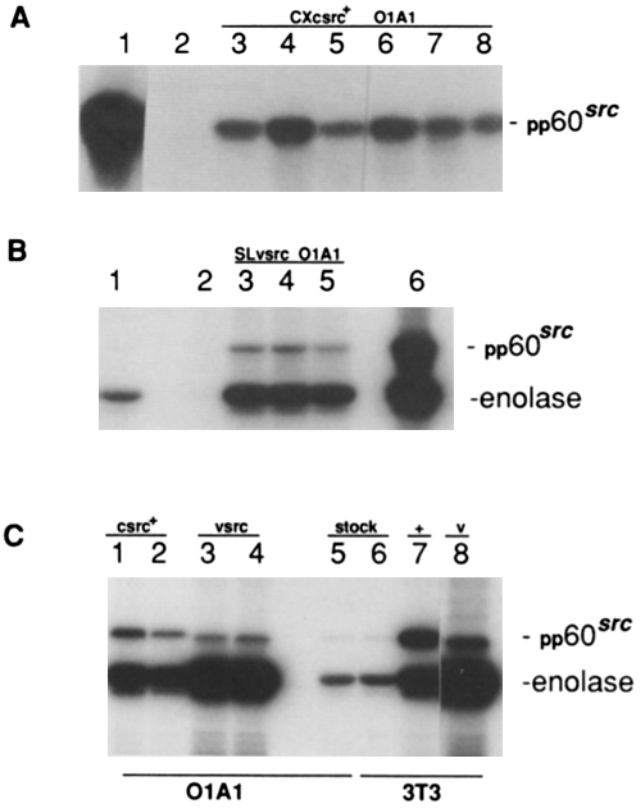

Figure 1. In vitro PTK activities of P19-O1A1 sublines. pp60^{src} was isolated from solubilized cell proteins by immunoprecipitation and reacted with ^{32}Pγ-ATP as described in Materials and Methods. NIH3T3 cells are shown for comparison in *A–C* (lanes *1*, *6*, and *6–8* respectively). mAb EC10 was used for lanes 2–6 in *B*. mAb 327 was used for *A* and *C* and lane 1 of *B*. (*A*) LNCXc-*src*$^+$ infected 3T3 cells (lane *1*), uninfected P19-O1A1 cells (lane *2*), cells from pooled LNCXc-*src*$^+$ G418 resistant colonies (lane *3*), and five LNCXc-*src*$^+$ sublines (lanes *4–8*). (*B*) Uninfected cells (lanes *1* and *2*), cells from pooled G418 resistant LNSL7v-*src* colonies (lane *3*), two LNSL7v-*src* sublines (lanes *4* and *5*), and LNSL7v-*src* infected 3T3 cells (lane *6*). (*C*) Gel for quantitation of in vitro PTK activities. LNCXc-*src*$^+$ sublines D and E (lanes *1* and *2*), LNSL7v-*src* sublines 4 and 3 (lanes *3* and *4*), P19-O1A1 stock cells (lane *5*), uninfected 3T3 cells (lane *6*), LNCXc-*src*$^+$ 3T3 cells (lane *7*), LNSL7v-*src* 3T3 cells (lane *8*). ^{32}P incorporation into enolase in lanes 7 and 8 was 31- and 72-fold higher than in lane 6. The exogenous substrate enolase was included in the phosphorylations for *B* and *C*. For *A–C*, all lanes are from the same autoradiogram; in *A* and *C* some intervening lanes were removed. pp60^{src} bands (some faint) could be seen in the original autoradiograms for all antibody 327 immunoprecipitates.

The relative levels of phosphotyrosine-containing proteins of stock, pp60$^{v\text{-}src}$–expressing, and pp60$^{c\text{-}src+}$–expressing P19 cells were determined by probing an immunoblot with a mAb that recognizes phosphotyrosine (Fig. 2 *B*). Expression of pp60$^{c\text{-}src+}$ does not result in a general elevation of phosphotyrosine levels in P19 cells (lane *2*), as expected from results obtained from over-expression of pp60$^{c\text{-}src}$ and pp60$^{c\text{-}src+}$ in other cell types (11, 25, 36). However, expres-

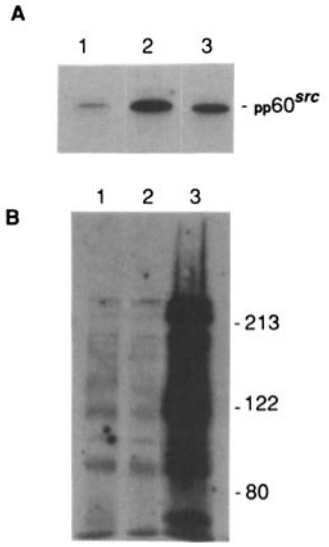

Figure 2. Levels of expression of pp60^{src} and detection of phosphotyrosine containing proteins in P19-OlA1 sublines. Cells from undifferentiated monolayer cultures of stock, subline SLvsrc3E, and subline CXcsrc^{+}E7 were solubilized with SDS buffer as described (20). 100 μg protein from each sample was resolved on a 10% (*A*) or 5% (*B*) acrylamide gel and then the region of the gel between the prestained ovalbumin and BSA standards (*A*) or the whole gel (*B*) was transferred to nitrocellulose. (*A*) Anti-pp60^{src} mAb 327 was used to detect pp60^{src} in stock P19-OlA1 cells (lane *1*), subline CXcsrc^{+}E7 (lane *2*), and subline SLvsrc3E (lane *3*). In two experiments, CXcsrc^{+}E7 cells had 7.8- and 7.9-fold more pp60^{src} than stock cells; SLvsrc3E cells had 4.8- and 5.5-fold more. Lanes 2 and 3 were reordered from the original autoradiogram to match the lane order in *B*. (*B*) Anti-phosphotyrosine mAb PY-20 was used to detect phosphotyrosine containing proteins of stock (lane *1*), subline CXcsrc^{+}E7 (lane *2*), and subline SLvsrc3E (lane *3*) cells. Positions of prestained molecular mass markers myosin (*213*), β-galactosidase (*122*), and BSA (*80*) are shown.

sion of pp60$^{v\text{-}src}$ caused a 25-fold elevation in phosphotyrosine levels (lane *3*).

The expression of pp60$^{v\text{-}src}$ and pp60$^{c\text{-}src+}$ does not cause a dramatic change in the morphology of P19 cells grown as monolayers (Fig. 3). Most of the cells in stock cultures adhere to each other in groups as "islands," while a minority are isolated (Fig. 3 *A*). Slight alterations in cell packing in the pp60$^{v\text{-}src}$– and pp60$^{c\text{-}src+}$–expressing P19 cell cultures were observed. The pp60$^{c\text{-}src+}$–expressing P19 cell lines had a slightly larger number of isolated cells (Fig. 3 *B*). Fewer pp60$^{v\text{-}src}$–expressing P19 cells grow as isolated cells, and the cells in islands are more evenly packed at the edges of the islands (Fig. 3 *C*). In contrast to non-RA-treated stock, pp60$^{v\text{-}src}$–expressing, and pp60$^{c\text{-}src+}$–expressing P19 cells, P19 cells exposed to RA as sparse monolayers have an altered morphology (Fig. 3 *D*). RA-treated P19 cells become flatter (phase dark) and more spread (1.6-fold more cells per unit area) on the culture surface. The subtle changes in cell packing observed for pp60$^{v\text{-}src}$– and pp60$^{c\text{-}src+}$–expressing P19 cells do not resemble the dramatic change in morphology observed after RA-induced differentiation.

We considered the possibility that pp60$^{v\text{-}src}$ and pp60$^{c\text{-}src+}$ expression could cause changes in the differentiation state of P19 cells in the absence of morphological changes. Embryonal carcinoma cells express embryonic antigens that are lost after differentiation. The effects of pp60$^{v\text{-}src}$ and pp60$^{c\text{-}src+}$ expression on P19 cell differentiation were assessed by immunofluorescence microscopy and antibody to stem cell marker SSEA-1 (Fig. 3, *E–H*). Most cells of P19 cultures that have not been exposed to RA express the SSEA-1 antigen (Fig. 3 *E*). RA treatment leads to the loss of expression of embryonic antigen SSEA-1 (Fig. 3 *H*), as previously

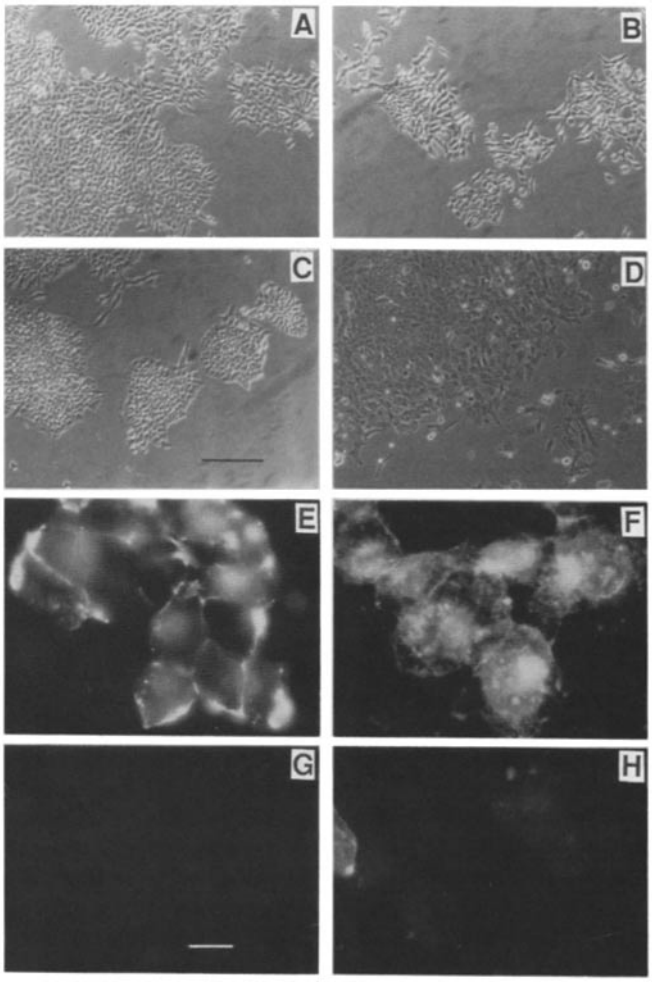

Figure 3. Morphology and SSEA-1 embryonic antigen of pp60$^{v\text{-}src}$- and pp60$^{c\text{-}src+}$-expressing P19-OlA1 cells. Morphology by phase-contrast microscopy of undifferentiated stock (*A*), pp60$^{c\text{-}src+}$-expressing (*B*), pp60$^{v\text{-}src}$-expressing (*C*), and differentiated stock P19-OlA1 cells from RA-treated monolayer culture (*D*). For *A–D*, cells were grown under normal culture conditions. For immunofluorescence detection of the SSEA-1 antigen, cells were grown on poly-D-lysine–coated coverslips. SSEA-1 embryonic cell antigen of undifferentiated stock (*E*), pp60$^{c\text{-}src+}$-expressing (*F*), pp60$^{v\text{-}src}$-expressing cells (*G*), and RA-treated monolayer culture cells (*H*). One cell that had not lost SSEA-1 expression in response to RA can be seen at the left edge of *H*. This cell had retained a rounded morphology and rested on top of flatter, SSEA-1-negative cells. Bars: (*A–D*) 200 μm; (*E–H*) 10 μm.

reported (48). SSEA-1 antigen expression is retained by pp60$^{c\text{-}src+}$–expressing P19 cells that are not exposed to RA (Fig. 3 *F*). In contrast, the pp60$^{v\text{-}src}$–expressing P19 cells do not express SSEA-1 antigen even in the absence of exposure to RA (Fig. 3 *G*).

Expression of pp60$^{c\text{-}src+}$ or pp60$^{v\text{-}src}$ Interferes with Neuronal Differentiation of P19 Cells

To examine the effects of pp60$^{c\text{-}src+}$ and pp60$^{v\text{-}src}$ on neuronal differentiation, stock, pp60$^{c\text{-}src+}$–expressing, and pp60$^{v\text{-}src}$–expressing P19 cell lines were induced to differentiate by exposing the cells to RA and allowing the cells to form extensive cell–cell contacts in floating aggregates. After 4 d, the

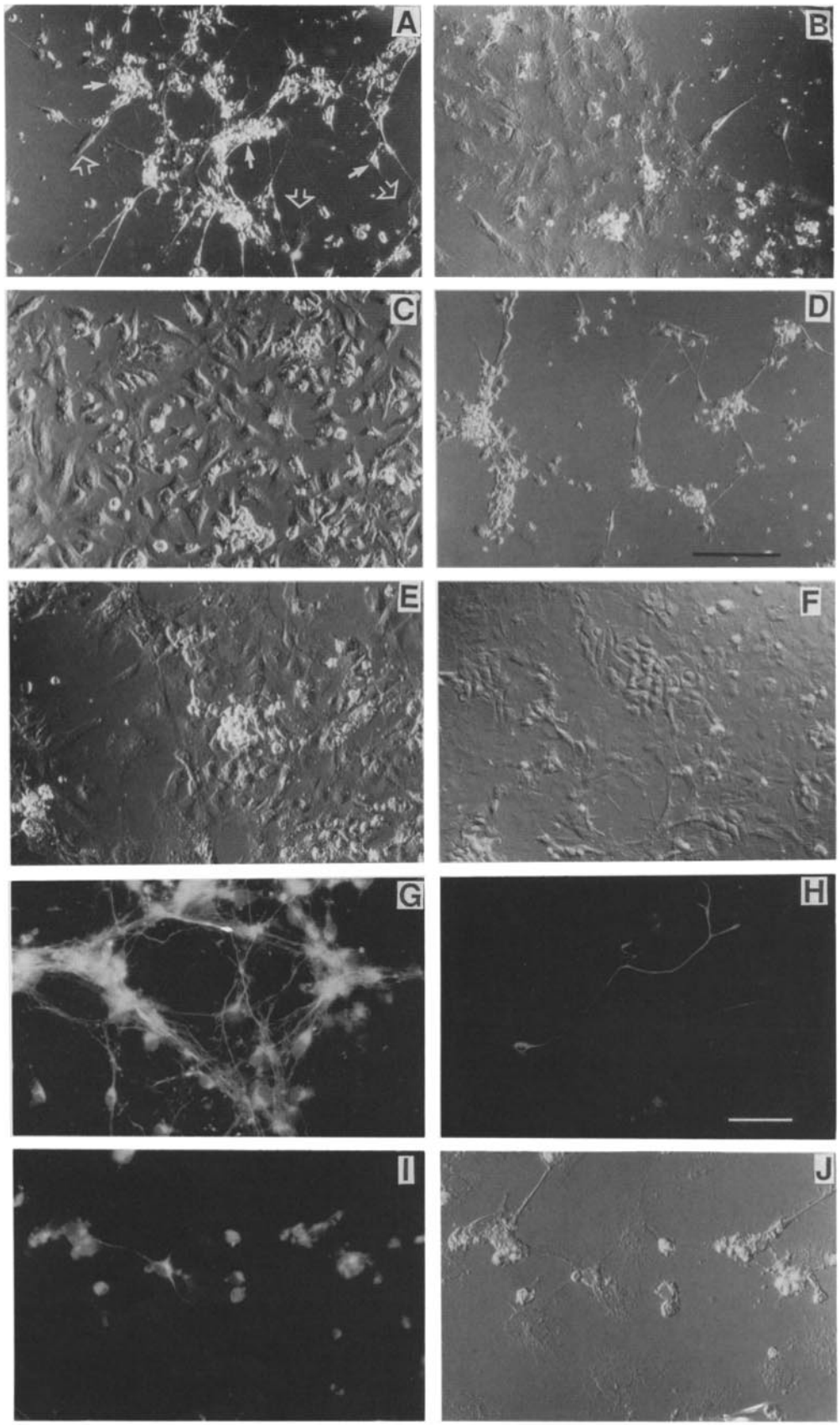

Figure 4. Morphology and NF-M of P19-O1A1 cells after neuronal differentiation. Morphology of P19 cells that had been treated for neural differentiation; stock (*A*), $pp60^{c\text{-}src+}$-expressing, (*B*) $pp60^{v\text{-}src}$-expressing cells (*C*), and G418 resistant (only) cells (*D*). Phase-bright, rounded, self-adhering (*closed arrows*) and phase-dark, flat (*open arrows*) cells are indicated in *A*. In *B* a region of a coverslip with few neuronal cells is shown: other areas on the same coverslip had more phase-bright cells. Stock P19 cells exposed to RA as sparse monolayers then aggregated and further processed as for neural differentiation (*E*). Stock cells that were RA treated and aggregated in low calcium (50 μM Ca^{++}) culture medium then processed for neuronal differentiation (*F*). Cells were fixed at 60 h (*A–F*) or 7 d (*G–J*) after disaggregation and culture on coverslips. Immunofluorescence detection of NF-M (*G–I*); stock P19 cells (*G*), $pp60^{v\text{-}src}$-expressing cells (*H*), $pp60^{c\text{-}src+}$-expressing cells (*I*), and corresponding Nomarsky image for *I* (*J*). For *I* and *J*, a sparse region of the coverslip is shown for easy identification of flat and round cells. For *H*, a dense region of the coverslip is shown which contained a rare cell with a neurofilament-positive process. Bars: (*A–F*) 100 μm; (*G–J*) 20 μm.

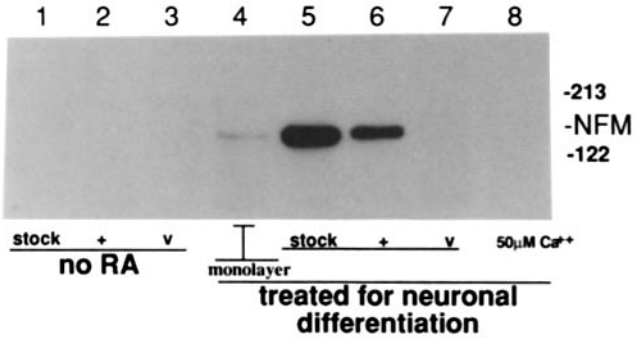

Figure 5. NF-M levels in P19-O1A1 cells. Cell proteins solubilized with SDS were resolved by SDS-PAGE and proteins in the region of the gel between the β-galactosidase (*122*) and myosin (*213*) prestained standards were transferred to nitrocellulose. NF-M (estimated M_r 143,000) was detected by probing the nitrocellulose with anti-NF-M antibody and ^{125}I-labeled protein A. Undifferentiated stock (lane *1*), pp60$^{c\text{-}src+}$-expressing (lane *2*), and pp60$^{v\text{-}src}$-expressing cells (lane *3*). Stock cells exposed to RA as sparse monolayers then treated as for neuronal differentiation (lane *4*). In three experiments these cells had 3, 5, and 3% of the NF-M level in stock cells. Cells treated according to the standard neuronal differentiation procedure for stock (lane *5*), pp60$^{c\text{-}src+}$-expressing (lane *6*), and pp60$^{v\text{-}src}$-expressing (lane *7*) P19 cells. In three experiments pp60$^{c\text{-}src+}$-expressing cells had 52, 87, and 53% of the NF-M level in stock cells; for pp60$^{v\text{-}src}$-expressing cells the values were <1, <1, and 7%. Stock P19 cells exposed to RA and aggregated in medium with 50 μM Ca^{++} and treated as for neuronal differentiation (lane *8*). In three experiments these cells had <1, <1, and 7% of the NF-M level in stock cells. Cells were harvested 11 d after exposure to RA.

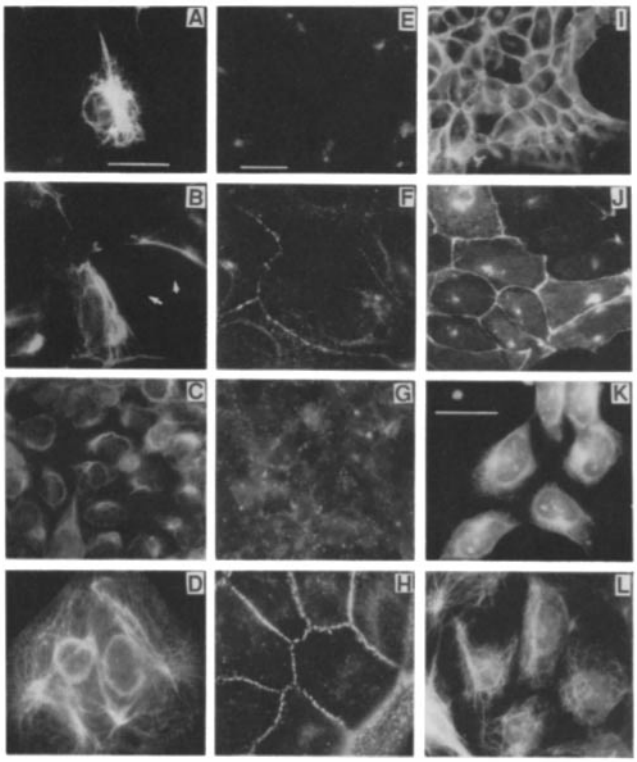

Figure 6. Immunofluorescence detection of cell-type markers. A glial fibrilary acidic protein-positive cell after neural differentiation of P19 cells (*A*). Cells were stained for Endo-A keratin filaments: P19 cells treated with RA in monolayer culture (*B* and *C*) and MDCK cells (*D*). The positions of two P19 cells that did not have detectable keratin filaments are indicated (*B*). Cells were stained for desmoplakins: undifferentiated P19 cells in monolayer culture (*E*), RA-treated P19 cells in monolayer culture (*F*), RA-treated and aggregated P19 cells (*G*), and MDCK cells (*H*). For *G*, aggregates were embedded and sectioned before staining. Cells were stained for E-cadherin: undifferentiated P19 cells (*I*) and P19 cells exposed to RA in sparse monolayer culture (*J*). Cells were stained for vimentin: stock P19 cells (*K*) or MDCK cells (*L*). Bars: (*A–D*) 20 μm; (*E–H*) 10 μm; (*I–L*) 20 μm.

aggregates were dissociated with trypsin and the cells plated in serum-free N2 medium (35). As previously reported, neuronal differentiation of stock P19 cells results in a characteristic morphology; self-adhering, rounded (phase bright) cell bodies with long processes (Fig. 4 *A*) (35, 44). Neurofilament expression (Fig. 4 *G* and Fig. 5, lane *5*) confirmed the identity of these cells as neurons. A small number of glial fibrilary acidic protein–positive cells are detected in these cultures (Fig. 6 *A*), as described (35). P19 sublines selected for resistance to G418 after infection with virus that does not include a *src* gene were found to undergo the characteristic neuronal differentiation (Fig. 4 *D*).

pp60$^{c\text{-}src+}$–expressing P19 sublines that were taken through the steps of the neuronal differentiation procedure showed an abnormal pattern of differentiation. Although many neurofilament-positive cells with long processes were present in these cultures, there were also many flat (Fig. 4 *B*), neurofilament-negative cells (Fig. 4 *I*). Very few of these spread, phase dark cell bodies were observed in the cultures of differentiated stock P19 cells (Fig. 4, *A* and *D*). Most differentiated pp60$^{v\text{-}src}$–expressing P19 cells have a flattened, nonneuronal morphology (Fig. 4 *C*). Very few neurofilament-positive cells (Fig. 4 *H*) or glial fibrilary acidic protein–positive cells (not shown) were detected in cultures of pp60$^{v\text{-}src}$–expressing P19 cells which were induced for neuronal differentiation. However, some partially rounded cell bodies with short extensions were present in these cultures. These cells did not have neurofilaments as determined by immunofluorescence (Fig. 4 *H*). P19 sublines selected for resistance to G418 after infection with a pLNCXc-*src* virus (expressing the nonneuronal pp60$^{c\text{-}src}$) also yielded more flat cells after the neuronal differentiation procedure than do stock P19 cells (not shown).

The levels of middle molecular weight neurofilament protein (NF-M) in non-RA-treated cultures of pp60$^{v\text{-}src}$– and pp60$^{c\text{-}src+}$–expressing P19 sublines were quantitated relative to the level in uninfected P19 cells (Fig. 5, lane *1*). Neither pp60$^{v\text{-}src}$ or pp60$^{c\text{-}src+}$ alone (Fig. 5, lanes *2* and *3*) induced expression of NF-M in the monolayer cultures, as reported previously for pp60$^{v\text{-}src}$ (5). Stock P19 cells differentiated as aggregates with RA displayed high levels of NF-M (Fig. 5, lane *5*). Cultures of differentiated pp60$^{c\text{-}src+}$–expressing P19 cells displayed a 36% reduction (Fig. 5, lane *6*) in NF-M protein relative to the stock cell level. In contrast, very low levels of NF-M protein were detected in differentiated cultures of pp60$^{v\text{-}src}$–expressing P19 sublines (3% of the stock cell level; Fig. 5, lane *7*). Thus, pp60$^{v\text{-}src}$ expression in undifferentiated P19 cells greatly decreases the capacity for RA-induced neuronal differentiation, as reported previously (5), and pp60$^{c\text{-}src+}$ expression interferes with neuronal differentiation in ~36% (based on NF-M levels) to 44% (based on

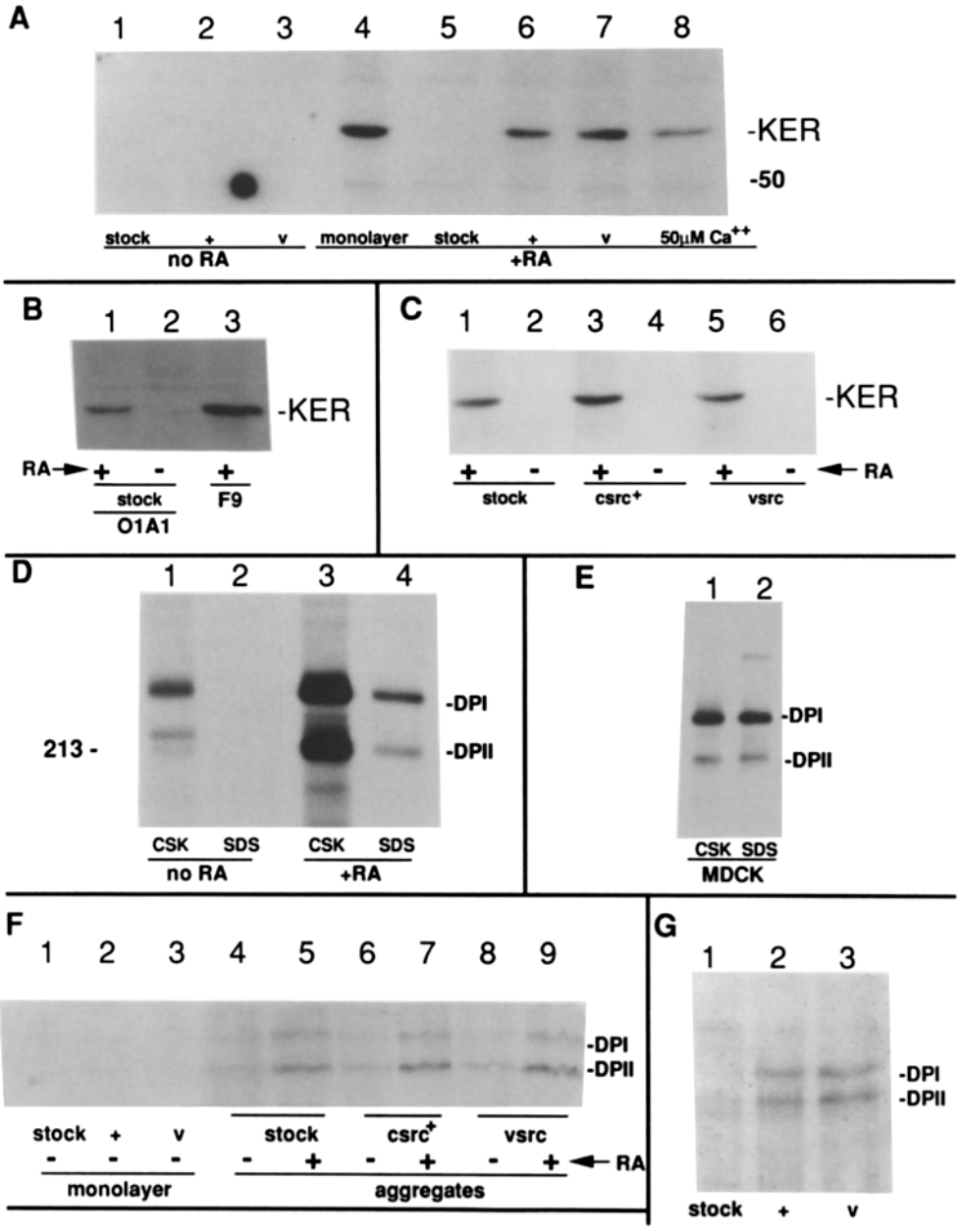

Figure 7. Keratin and desmoplakin expression in P19-O1A1 cells. Cell proteins solubilized as described in Materials and Methods were resolved by SDS-PAGE and transferred to nitrocellulose. Keratin and desmoplakins were detected by probing the nitrocellulose with antikeratin or antidesmoplakin antibodies and ^{125}I-labeled protein A followed by autoradiography (*A*, *B*, *C*, *F*, and *G*). For *D* and *E*, metabolically labeled desmoplakins were immunoprecipitated, resolved by SDS-PAGE, and visualized by autoradiography. (*A*) Undifferentiated stock (lane *1*), pp60$^{c\text{-}src+}$-expressing (lane *2*), pp60$^{v\text{-}src}$-expressing (lane *3*) P19 cells. Stock P19 cells in sparse monolayer culture exposed to RA and then treated as for neuronal differentiation (lane *4*). Cultures processed for neuronal differentiation; stock (lane *5*), pp60$^{c\text{-}src+}$-expressing (lane *6*), pp60$^{v\text{-}src}$-expressing (lane *7*), and stock P19 cells aggregated in 50 μM Ca^{++} and treated as for neuronal differentiation (lanes *8*). For lanes 4–8 cells were harvested 11 d after exposure to RA. (*B*) Comparison of keratin levels in RA-treated monolayer P19-O1A1 cells (lane *1*), non-RA-treated P19-O1A1 cells (lane 2), and RA-treated monolayer cultures of F9 cells (lane *3*. (*C*) Comparison of keratin levels in 2-d P19 cell aggregates: RA-treated (lanes *1*, *3*, and *5*) and non-RA-treated (lanes *2*, *4*, and *6*). Stock (lanes *1* and *2*), pp60$^{c\text{-}src+}$-expressing (lanes *3* and *4*), pp60$^{v\text{-}src}$-expressing (lanes *5* and *6*) cells. (*D*) ^{35}S-methionine-labeled (3-h labeling) stock P19 cells grown for 2 d as floating aggregates. Detection of DPI and DPII in CSK-soluble (lane *1*) and CSK-resistant (lane *2*) fractions of aggregates grown in the absence of RA. DPI and DPII in CSK-soluble (lane *3*) and CSK-resistant (lane *4*) fractions of RA-treated cells. Approximately equal numbers of cells were labeled and incorporation of ^{35}S-methionine into total protein was similar for aggregates with and without RA. The solubilized protein samples were split in half and also used for Fig. 9 *F*. (*E*) Comparison of desmoplakins in CSK-soluble (lane *1*) and CSK-resistant (lane *2*) fractions of ^{35}S-methionine-labeled (2-h labeling) MDCK cells. (*F*) Desmoplakin levels in non-RA-treated monolayer cultures of stock (lane *1*), pp60$^{c\text{-}src+}$-expressing (lane *2*), and pp60$^{v\text{-}src}$-expressing (lane *3*) cells. Desmoplakin levels in RA-treated (lanes *5*, *7*, and *9*) and non-RA-treated (lanes *4*, *6*, and *8*) 2-d-old aggregates of stock (lanes *4* and *5*) of pp60$^{c\text{-}src+}$-expressing (lanes *6* and *7*) and pp60$^{v\text{-}src}$-expressing (lanes *8* and *9*) cells. (*G*) Desmoplakin levels in P19 cultures processed for neuronal differentiation: stock (lane *1*), pp60$^{c\text{-}src+}$-expressing (lane *2*), and pp60$^{v\text{-}src}$-expressing (lane *3*) cells. Cells were harvested 11 d after exposure to RA. Gels were 10% or 5% acrylamide for keratin (*KER*) or DPI and DPII, respectively. Positions of prestained protein standards myosin (*213*) and ovalbumin (*50*) are indicated in *D* and *A*, respectively.

keratin levels, see below) of the population. The presence of the phase-dark, flattened cells in both the pp60$^{c\text{-}src+}$– and pp60$^{v\text{-}src}$–expressing cell cultures suggested that these PTKs directed differentiation towards a nonneural lineage.

Expression of pp60$^{c\text{-}src+}$ or pp60$^{v\text{-}src}$ Does Not Prevent Epithelial Differentiation of P19 Cells

The flattened, nonneuronal cells in cultures of RA-treated pp60$^{v\text{-}src}$– and pp60$^{c\text{-}src+}$–expressing P19 sublines (Fig. 4, *B* and *C*) morphologically resemble the nonneuronal cells obtained by exposing stock P19 cells in sparse monolayer culture to RA (Fig. 4 *E*). Cells with a flattened morphology and keratin intermediate filaments have previously been identified in P19 monolayer cultures after exposure to RA (48). This suggested that the pp60$^{v\text{-}src}$– and pp60$^{c\text{-}src+}$–expressing P19 cells might have undergone epithelial differentiation in

response to RA under conditions that give neuronal differentiation of stock cells. The epithelial differentiation of these cells was characterized by analyzing the expression of desmosomal proteins desmoplakins I and II (55) and keratin intermediate filaments as markers of epithelial differentiation. Keratins are components of intermediate filaments in epithelial cells and they are found together with desmosomes only in epithelial cells (47). The epithelial differentiation of P19 cells exposed to RA in sparse monolayer culture was also characterized for comparison.

We examined expression of keratin with the mAb TROMA-1, which has previously been shown to react with keratin in P19 monolayers treated with RA (48). Immunofluorescence (Fig. 6) and immunoblot assays (Fig. 7) were used to examine keratin expression. Non-RA-treated P19 cells have a very low level of keratin (Fig. 7 *A*, lane *1*). After RA treatment of monolayer P19 cultures, keratin filaments can be detected in some of the cells (Fig. 6, *B* and *C*), as previously reported (48). The increase in mAb TROMA-1-reactive keratin (estimated M_r 56,000) protein after RA treatment of P19 cells in sparse monolayer culture is shown in Fig. 7 *B* (lanes *1* and *2*).

Most of the RA-treated P19 cells (Fig. 6 *C*) have relatively few keratin filaments. Unlike RA-treated F9 cells (32), not all of the RA-treated P19 cells that take on a flattened morphology have detectable keratin filaments (Fig. 6 *B*). RA-treated F9 cells (Fig. 7 *B*, lane *3*) have a higher level of TROMA-1-reactive keratin than P19 cells (Fig. 7 *B*, lane *1*). The keratin filaments that we detect in flat, nonneuronal, differentiated P19 cells (Fig. 6, *B* and *C*) are often not as uniformly dispersed throughout the cytoplasm as in RA-treated F9 embryonal carcinoma cells (24) or MDCK cells (Fig. 6 *D*). The keratin filaments of many RA-treated P19 cells are present in clumps mostly on one side of the nuclei rather than as a well dispersed network throughout the cells.

Cultures of stock P19 cells that have undergone neuronal differentiation do not have a detectable (by Western blot) level of keratin (Fig. 7 *A*, lane *5*), although a very small number of cells in these cultures have keratin filaments detectable by immunofluorescence (not shown). Expression of $pp60^{c\text{-}src+}$ or $pp60^{v\text{-}src}$ in P19 cells maintained without RA treatment does not induce keratin expression (Fig. 7 *A*, lanes *2* and *3*), as reported previously for $pp60^{v\text{-}src}$ (5). However, like stock P19 cells (Fig. 7 *B*, lane *1*), cells of $pp60^{c\text{-}src+}$– or $pp60^{v\text{-}src}$–expressing sublines express keratin after exposure to RA in monolayer culture (not shown) or when grown as floating aggregates and treated for neuronal differentiation (Fig. 7 *A*, lanes *6* and *7*). Unlike stock cells, $pp60^{c\text{-}src+}$– and $pp60^{v\text{-}src}$–expressing P19 cells continue to express keratin under conditions which in stock P19 cells result in neurofilament expression and very little keratin expression.

Desmoplakins are cytoplasmic, structural proteins of desmosomes (55). Desmoplakin expression was analyzed by immunofluorescence (Fig. 6) and by immunoblot and metabolic labeling (Fig. 7). In undifferentiated P19 cells, antidesmoplakin antibodies reveal diffuse staining in a peri-nuclear region of the cytoplasm (Fig. 6 *E*). After RA treatment of P19 cells in monolayer culture, most of the peri-nuclear stain is dispersed and punctate staining is detected inside cells and at sites of cell-cell contacts (Fig. 6 *F*). The level of ^{35}S-methionine incorporated into desmoplakins is increased (12-fold in Fig. 7 *D*, lane *3*) in stock P19 cells after RA exposure as compared to non-RA-treated P19 cells (Fig. 7 *D*, lane *1*). After RA treatment, stock P19 cells have a higher level of desmoplakins I and II (DPI and DPII) and a fraction of these desmosomal components is resistant to extraction in buffer (CSK; see Materials and Methods) containing nonionic detergent (Fig. 7 *D*, lane *4*). These extraction conditions have previously been used to demonstrate a correlation between the pool of desmoplakins that is resistant to solubilization with nonionic detergent (CSK resistant) and assembly into desmosomes (55). Compared to MDCK cells (Fig. 7 *E*), the P19 cells do not efficiently recruit DPI and DPII into the CSK-resistant pool. This difference in recruitment correlates with a higher density of cell–cell interface localized desmoplakin staining of MDCK cells (Fig. 6 *H*). These results are consistent with RA-induced stabilization of some desmoplakins at cell surface desmosomes between adjacent P19 cells.

Like stock P19 cells, the $pp60^{v\text{-}src}$– and $pp60^{c\text{-}src+}$–expressing P19 cells also have elevated levels of desmoplakins after exposure to RA (Fig. 7 *F*). However, in contrast to stock P19 cells, the cells of $pp60^{v\text{-}src}$–expressing and $pp60^{c\text{-}src+}$–expressing P19 sublines have detectable desmoplakin expression 11 d after exposure to RA (Fig. 7 *G*, lanes *2* and *3*) under conditions that induce neuronal differentiation and little desmoplakin expression in stock P19 cells (Fig. 7 *G*, lane *1*). The expression of keratin and desmoplakins in $pp60^{v\text{-}src}$–expressing and $pp60^{c\text{-}src+}$–expressing P19 cells correlates with the appearance of flat, nonneuronal cells in these cultures under conditions that give neuronal differentiation of stock P19 cells.

Thus, while not all of the nonneuronal, RA-treated P19 cells express detectable keratin filaments and desmosomes, a large percentage of the cells do have desmosomes (above) and keratin filaments, as described previously (48). These flat, nonneuronal, differentiated P19 cells display heterogeneity in morphology (extent of cell spreading on the substrate) and expression of keratin filaments and desmosomes. Heterogeneity of nonneural RA-treated P19 cells has been previously described (48, 50, 59). Low levels of RA have been used to induce muscle cells in P19 cultures (16). Using immunofluorescence, the muscle-specific intermediate filament protein desmin has not been detected in our P19 cultures. The intermediate-sized filament component vimentin is detected in non-RA-treated P19 cells (Fig. 6 *K*), but the staining is diffuse rather than filamentous (Fig. 6 *L*), as previously reported (17). The vimentin staining in P19 cells is concentrated in a compact region to one side of the cell nuclei.

Based on results with the marker proteins, we conclude that $pp60^{v\text{-}src}$ or $pp60^{c\text{-}src+}$ expression alone does not result in neuronal or epithelial differentiation of P19 cells. However, expression of $pp60^{v\text{-}src}$ in P19 cells does result in the loss of SSEA-1 embryonic antigen. Our results agree with the conclusion of Boulter and Wagner (5) that $pp60^{v\text{-}src}$–expressing P19 cells lose expression of stem cell markers but do not commit to a complete differentiation program. Our results with the epithelial markers show that $pp60^{v\text{-}src}$– and $pp60^{c\text{-}src+}$–expressing P19 cells can respond to RA by differentiating and attaining an epithelial phenotype.

Transient Expression of an Epithelial Phenotype in Retinoic Acid–treated and Aggregated Stock P19 Cells

The expression of an epithelial phenotype of $pp60^{v\text{-}src}$– and

$pp60^{c\text{-}src}$–expressing P19 cells in long term cultures induced with RA under the conditions for neuronal differentiation prompted us to test for an epithelial phenotype in cells of stock P19 aggregates. RA exposure results in a rapid increase in keratin levels in floating aggregates of stock, $pp60^{v\text{-}src}$–expressing, and $pp60^{c\text{-}src+}$–expressing P19 sublines (Fig. 7 *C*). Aggregated cells of stock, $pp60^{v\text{-}src}$–expressing, and $pp60^{c\text{-}src+}$–expressing P19 sublines also respond rapidly to RA by increasing levels of desmoplakin protein (Fig. 7, *D* and *F*). P19 cells and RA-treated aggregates have punctate desmoplakin staining throughout the entire thickness of the aggregates (Fig. 6 *G*) and CSK-resistant desmoplakin (Fig. 7 *D*, lane *4*). Stock P19 cells only transiently express an epithelial phenotype during the aggregation stage of the neuronal differentiation procedure. After disaggregation and culture in N2 medium most stock P19 cells differentiate into neurons and lose keratin and desmoplakin expression.

Expression of $pp60^{c\text{-}src+}$ or $pp60^{v\text{-}src}$ Reduces Cell–Cell Adhesion in Retinoic Acid–treated P19 Cell Aggregates

Efficient neural differentiation of P19 cells is achieved by allowing the cells to form floating aggregates during exposure to RA. Stock P19 cells form tightly compacted aggregates under these conditions (Fig. 8 *A*). As seen by phase-contrast microscopy, the surface of well compacted aggregates is smooth with few protruding cells. In contrast, $pp60^{v\text{-}src}$–expressing (Fig. 8 *C*) and $pp60^{c\text{-}src+}$–expressing (Fig. 8 *B*) P19 cell aggregates are less tightly compacted and individual cell bodies are more protrusive on the surfaces of the aggregates. While stock P19 cell aggregates occasionally adhere to the bacteriological grade culture dishes, such adherence was more prevalent in the $pp60^{v\text{-}src}$–expressing cell cultures. After RA treatment and aggregation, those $pp60^{v\text{-}src}$–expressing P19 cells that adhered to the culture dish could be seen to have short processes (Fig. 8 *C*, *inset*). These processes are similar to those observed in other nonneural $pp60^{v\text{-}src}$–expressing cells such as MDCK cells (69). Interestingly, the decrease in compaction for aggregates of $pp60^{c\text{-}src+}$– and $pp60^{v\text{-}src}$–expressing P19 cells is observed only in RA-treated aggregates (compare Fig. 8, *E* and *F*).

Cell aggregation was quantitated in a reaggregation assay (Fig. 8 *G*). Cells were exposed to RA and allowed to form floating aggregates for 2 d in medium with a lower than normal concentration of calcium (50 μM Ca^{++}). Under these conditions the aggregates are not compacted and the cells were disassociated by trituration. The cells were then transferred to medium with a normal, high level of Ca^{++} (1.8 mM). The percentage of cells with extensive cell–cell contacts was determined by phase contrast microscopy (see Fig. 8, legend) at times from 0 to 24 h after return to 1.8 mM Ca^{++}. The $pp60^{c\text{-}src+}$– and $pp60^{v\text{-}src}$–expressing P19 cells have slower rates of compaction than stock cells and they do not attain as high a percentage of compaction by 24 h (Fig. 8 *G*). The rates of compaction during the first 8 h for $pp60^{c\text{-}src+}$– and $pp60^{v\text{-}src}$–expressing P19 cells were 62 and 31% of the stock cell rate, respectively.

A cell–cell contact requirement for neural differentiation of P19 cells has previously been indicated by comparison of RA-treated cells from aggregates and sparse monolayer cultures (28). Most stock P19 cells exposed to RA as monolayers and then taken through the remaining steps of the neuronal differentiation procedure have a nonneuronal morphology (Fig. 4 *E*), however, some cells with neuronal morphology were observed. The extent of neuronal differentiation attained under these conditions of limited cell-cell contact during exposure to RA was quantitated in terms of NF-M expression. Cultures of these cells have a low level of NF-M (4% of the level in stock P19 cells; Fig. 5, lane *4*) and respond to RA by expressing keratin (Fig. 7 *A*, lane *4*). The decreased neural differentiation and cell–cell adhesion in aggregates of RA-treated $pp60^{v\text{-}src}$–expressing and $pp60^{c\text{-}src+}$–expressing P19 cells and the fact that these aggregated cells have an epithelial phenotype suggested that a cell–cell adhesion protein of epithelial cells (such as E-cadherin) might play a critical role in the neural differentiation of P19 cells.

Inhibition of normal P19 cell–cell contacts by formation of mixed aggregates with RA-non-responsive cells has previously been shown to inhibit neural differentiation in RA-treated aggregates (9). In similar experiments, we have taken advantage of the fact that the cell–cell adhesion function of cadherins can be blocked by lowering the extracellular Ca^{++} concentration. Stock P19 cells exposed to RA and allowed to aggregate in medium containing 50 μM Ca^{++} do not form tightly compacted aggregates (Fig. 8 *D*). The decreased compaction of aggregates formed by RA-treated $pp60^{v\text{-}src}$– and $pp60^{c\text{-}src+}$–expressing P19 cells in 1.8 mM Ca^{++} is not as extreme as for stock P19 cells aggregated in 50 μM Ca^{++}. Stock P19 cells exposed to RA and aggregated in 50 μM Ca^{++}, but otherwise treated for neuronal differentiation, have a nonneuronal morphology (Fig. 4 *F*) and a low level of NF-M (2% of the level in stock cells; Fig. 5, lane *8*). P19 cells in the noncompacted aggregates formed in 50 μM Ca^{++} respond to RA by expressing keratin (Fig. 7 *A*, lane *8*). These results suggest that an extracellular calcium-dependent system may be required during the aggregation phase of the neuronal differentiation process in order to achieve neuronal differentiation.

E-cadherin in P19 Cells

The altered cell–cell packing of $pp60^{c\text{-}src+}$– and $pp60^{v\text{-}src}$–expressing P19 cells suggested that expression of the cell adhesion molecule E-cadherin might be altered in these cells. Immunofluorescence reveals E-cadherin staining at cell–cell contacts of undifferentiated (Fig. 6 *I*) and RA-treated P19 cells (Fig. 6 *J*). Determination of total E-cadherin levels by Western blot shows that undifferentiated F9 embryonal carcinoma cells (1) and P19 cells have high levels of E-cadherin (Fig. 9 *A*, lanes *1* and *2*). The level of total E-cadherin in non-RA-treated P19 monolayer cultures is greater (12-fold greater in Fig. 9 *A*, lane *2*) than the level in cultures that had been exposed to RA (Fig. 9 *A*, lane *3*), in agreement with the recent report that levels of E-cadherin mRNA are decreased after exposure of cells to RA (49). The relative levels of total cell E-cadherin in cultures of stock, $pp60^{c\text{-}src+}$–expressing and $pp60^{v\text{-}src}$–expressing P19 cells were determined. Compared to stock P19 cells (Fig. 9 *B*, lane *1*), $pp60^{c\text{-}src+}$–expressing P19 cells have a lower amount of E-cadherin (65%; Fig. 9 *B*, lane *2*). In contrast, slightly more E-cadherin is present in $pp60^{v\text{-}src}$–expressing P19 cells (1.2-fold more than stock cells; Fig. 9 *B*, lane *3*).

Levels of E-cadherin present on the cell surface were determined by trypsinization of E-cadherin at the cell surface which gives rise to a large extracellular domain fragment

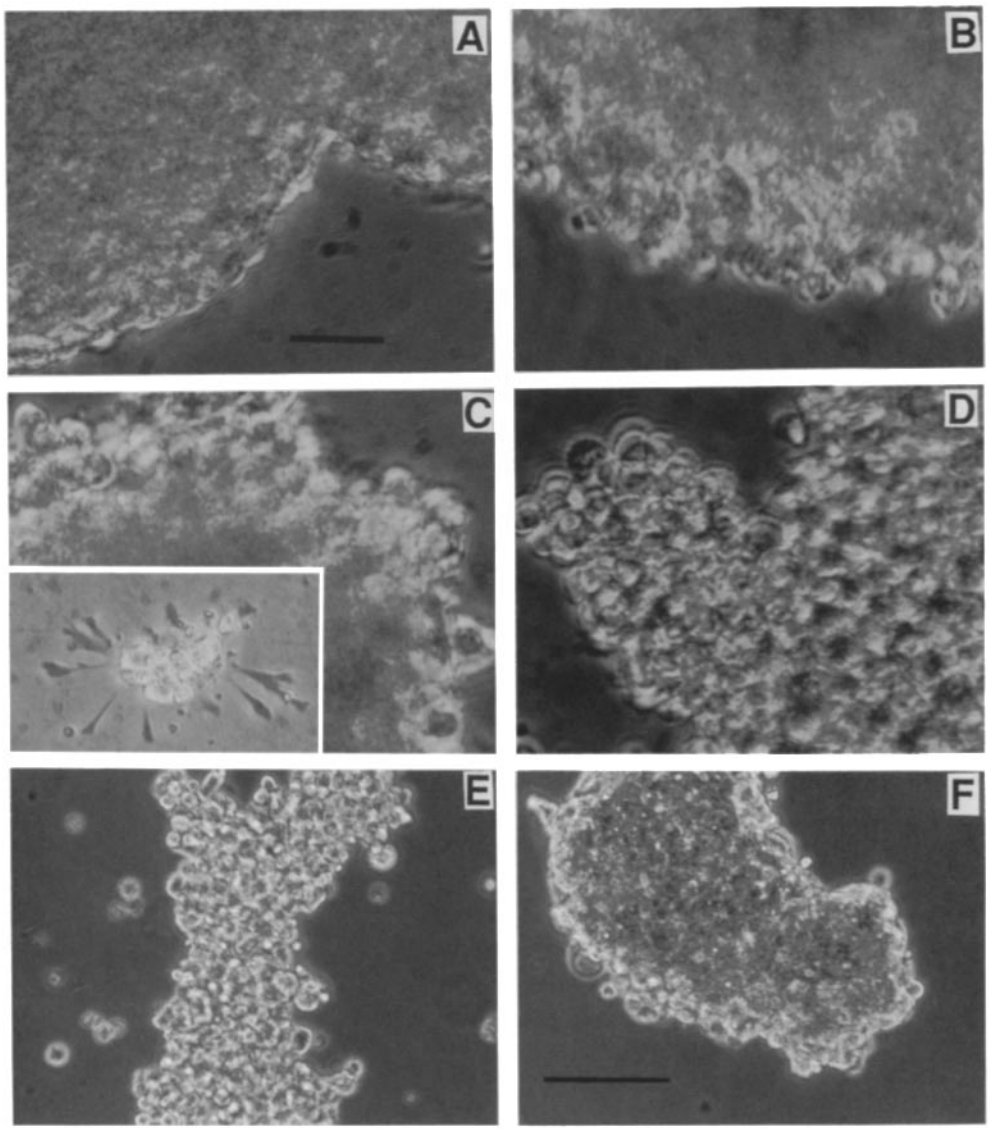

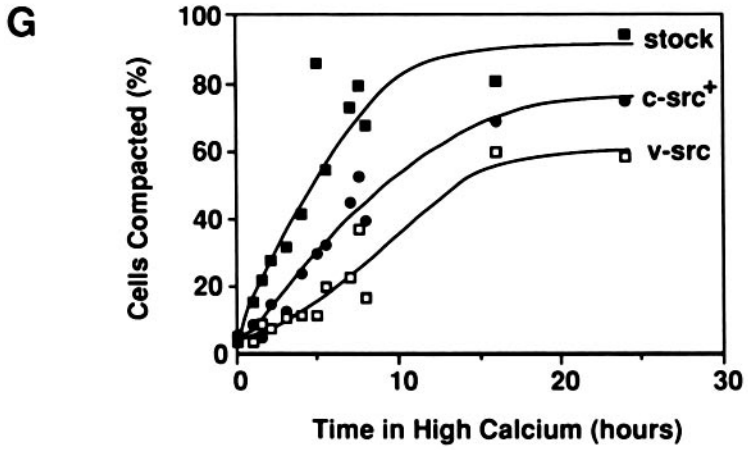

Figure 8. Decreased compaction of aggregates formed by retinoic acid–treated pp60$^{c\text{-}src+}$ and pp60$^{v\text{-}src}$-expressing P19 cells. Undifferentiated cells were allowed to form floating aggregates for 2 d in the presence of RA (*A–D*). Phase-contrast images of large aggregates in culture dishes: stock P19 cells (*A*), pp60$^{c\text{-}src+}$-expressing cells (*B*), pp60$^{v\text{-}src}$-expressing cells (*C*), and stock P19 cells in medium with 50 μM Ca^{++} (*D*). A small pp60$^{v\text{-}src}$-expressing cell aggregate that attached to the dish with short extensions (*C, inset*). For *E* (with RA) and *F* (no RA) pp60$^{c\text{-}src+}$-expressing cell aggregates were photographed after mounting on slides under coverslips. (*G*) Time course of compaction of RA-treated stock (■), pp60$^{c\text{-}src+}$-expressing (●), and pp60$^{v\text{-}src}$-expressing (□) P19 cells. Cells were grown for 2 d in bacteriological grade culture dishes in medium with RA and 50 μM Ca^{++}. The cells were transferred to medium with 1.8 mM Ca^{++} at time zero and cultured for up to an additional 24 h as floating aggregates. The percentage of cells which had formed close cell–cell contacts (compacted) was determined by triturating the aggregates, mounting aliquots on a hemocytometer, and counting compacted and noncompacted cells as viewed by phase-contrast microscopy. In compacted aggregates individual cells were difficult to discern (*F*) while in noncompacted aggregates the borders between individual cells appear as phase-bright rings (*E*). Under the conditions for this reaggregation assay the resulting small aggregates were similar to those shown by Littlefield (40) in his Fig. 4 (A and B) and individual compacted and noncompacted cells could be counted. The data points from three separate experiments (each of which included the three cell types) were combined for this graph. Bars: (*A–D*) 50 μm; (*E* and *F*) 100 μm.

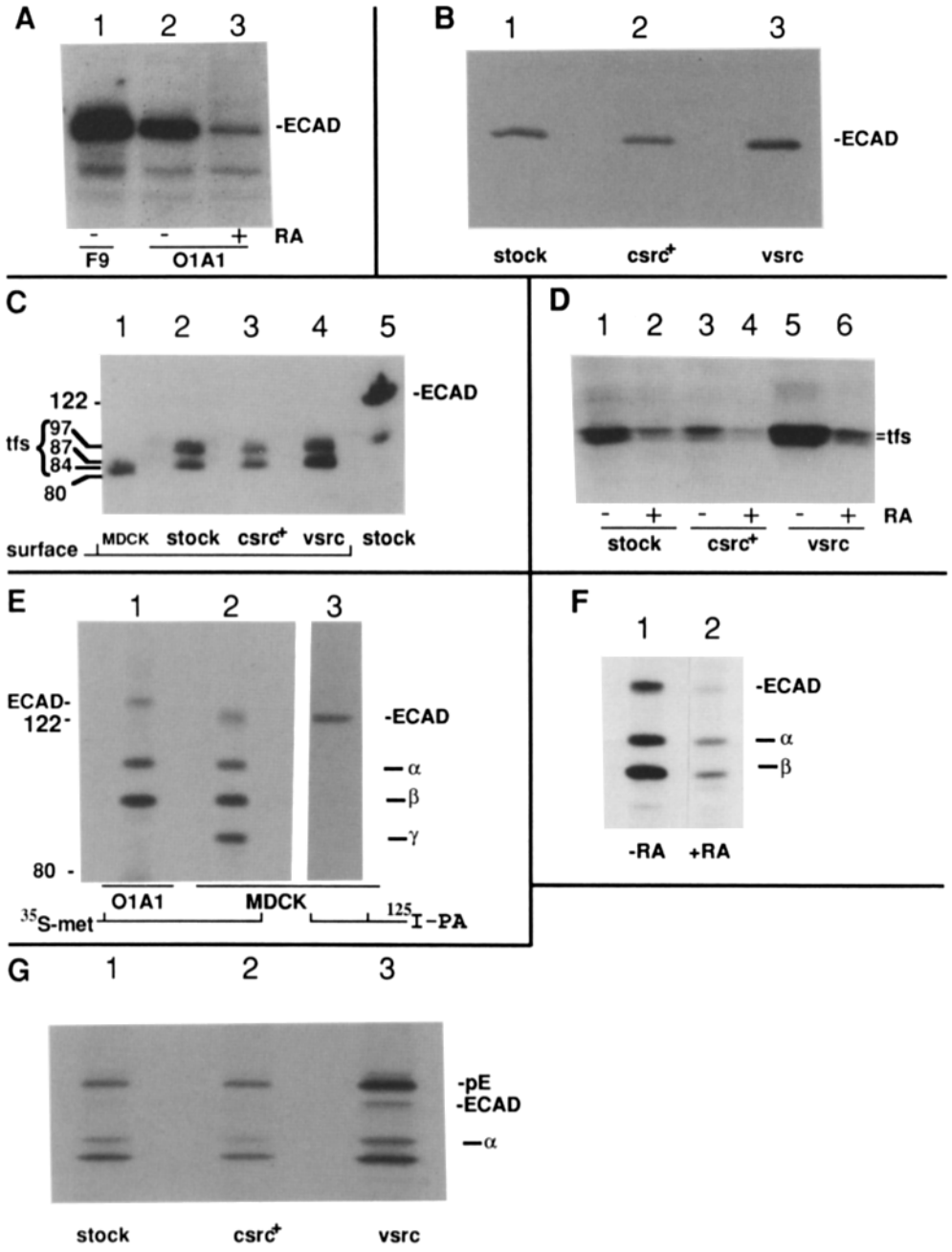

Figure 9. E-cadherin in P19-O1A1 cells. For *A* and *B* cells were solubilized with RIPA buffer and equal amounts of solubilized protein for each sample were resolved by SDS-PAGE and transferred to nitrocellulose. The pieces of nitrocellulose were probed with anti-E-cadherin antiserum and ^{125}I-labeled protein A. (*A*) Levels of E-cadherin in undifferentiated F9 cells (lane *1*), and undifferentiated P19-O1A1 cells in monolayer culture (lane *2*). P19-O1A1 cells exposed to RA as sparse monolayers (harvested 5 d after exposure to RA; lane *3*). (*B*) E-cadherin levels in stock (lane *1*), pp60$^{c\text{-}src+}$-expressing (lane *2*), and pp60$^{v\text{-}src}$-expressing (lane *3*) undifferentiated P19 cell monolayers. (*C*) E-cadherin levels at the surface of stock (lane *2*), pp60$^{c\text{-}src+}$-expressing (lane *3*), pp60$^{v\text{-}src}$-expressing (lane *4*) undifferentiated P19 cells. For lanes 2–4 approximately equal numbers of cells were processed for detection of cell surface E-cadherin as described in Materials and Methods. The positions of the 84-, 87-, and 97-kD E-cadherin extracellular domain tryptic fragments (*tfs*) are shown. In three experiments the level of cell surface E-cadherin on pp60$^{c\text{-}src+}$-expressing cells was 50, 45, and 54% of the level on stock cells; pp60$^{v\text{-}src}$-expressing cells had 1.3-, 1.65-, and 1.07-fold more surface E-cadherin than stock cells. Cell surface MDCK E-cadherin fragment (lane *1*). P19 E-cadherin, not trypsinized (lane *5*). (*D*) Cell surface E-cadherin in aggregated P19 cells. 2-d aggregates without (lanes *1*, *3*, and *5*) or with RA (lanes *2*, *4*, and *6*). Control (lanes *1* and *2*), pp60$^{c\text{-}src+}$-expressing (lanes *3* and *4*), pp60$^{v\text{-}src}$-expressing cells (lanes *5* and *6*). (*E–G*) ^{35}S-methionine metabolic labeling of E-cadherin. Cultures were labeled by growth in ^{35}S-methionine containing medium for 15 min (*G*), 2 h (*E*), or 3 h (*F*). Cells were solubilized with CSK buffer and CSK-solubilized proteins that were immunoprecipitated by anti-E-cadherin antiserum are shown. The indicated bands migrate at the positions of E-cadherin and the coprecipitating α, β, and γ catenins. Fluorographic autoradiography for immunoprecipitates resolved by SDS-PAGE is shown. (*E*) Stock (no RA) aggregated P19 cells (lane *1*) or MDCK cells (lane *2*). (Lane *3*) MDCK cell proteins were solubilized with CSK buffer, resolved by SDS-PAGE, transferred to nitrocellulose, and probed with anti-E-cadherin antiserum. (*F*) Stock P19 cells were grown as floating aggregates for 2 d then labeled; non-RA-treated cells (lane *1*) and cells exposed to RA (lane *2*). Approximately equal numbers of cells were labeled and incorporation of ^{35}S-methionine into total protein was similar for lanes 1 and 2. These samples were split in half and also used for Fig. 7 *D*. All E-cadherin was CSK soluble (not shown). These lanes are from the same autoradiogram; some intervening lanes were removed. (*G*) Cells in monolayer culture without RA were labeled: stock (lane *1*), pp60$^{c\text{-}src+}$-expressing (lane *2*), and pp60$^{v\text{-}src}$-expressing cells (lane *3*). pE indicates the position of the E-cadherin precursor. Gels were 5% (*E* and *F*) or 7.5% acrylamide. The positions of prestained size markers β-galactosidase (*122*) and BSA (*80*) are shown for some parts.

(66). Mature E-cadherin in P19 cells has an apparent M_r of 129,000 (Fig. 9 *C*, lane *5*). Trypsin digestion of MDCK cells in the presence of calcium releases an 84,000-D, trypsin-resistant, extracellular domain fragment of E-cadherin that can be detected with antibodies that recognize the extracellular domain of E-cadherin (Fig. 9 *C*, lane *1*). Trypsin digestion of P19 cells in monolayer culture (Fig. 9 *C*, lanes *2–4*) releases fragments ranging from 87,000 to 97,000 D. These multiple

bands are probably partially digested fragments. These fragments react with the antiserum which recognizes the extracellular domain of E-cadherin and were used to quantitate the cell surface E-cadherin of P19 cells. Compared to stock P19 cells (Fig. 9 *C*, lane *2*), less E-cadherin is detected on the surface of pp60$^{c\text{-}src+}$-expressing P19 cells (50%; Fig. 9 *C*, lane *3*). In contrast, more E-cadherin is present on the surface of pp60$^{v\text{-}src}$-expressing P19 cells (1.3-fold more than stock cells; Fig. 9 *C*, lane *4*).

E-cadherin expression in P19 cells was also analyzed by metabolic labeling. E-cadherin has previously been shown to coprecipitate with three lower molecular weight proteins called α, β, and γ catenin (53). ^{35}S-methionine-labeled E-cadherin and three associated proteins were coimmunoprecipitated from MDCK cells (Fig. 9 *E*, lane *2*). Only E-cadherin reacts with this antiserum (lane *3*), as described previously (53). E-cadherin from mouse cells (Fig. 9 *E*, lane *1*) has a slightly lower electrophoretic mobility than that of E-cadherin from MDCK cells (129 and 124 kD, respectively). Proteins migrating at the positions of the α and β catenins predominate in P19 cells. The lower level of E-cadherin in RA-treated P19 cells (Fig. 9 *A*) correlated with decreased ^{35}S-methionine incorporation into E-cadherin (Fig. 9 *F*).

The relative differences in E-cadherin levels of pp60$^{v\text{-}src}$- and pp60$^{c\text{-}src+}$-expressing P19 cells (Fig. 9 *B*) were also detected in metabolic labeling experiments (Fig. 9 *G*). In a 15-min pulse-labeling experiment, pp60$^{v\text{-}src}$-expressing P19 cells synthesized more (2.8-fold more; Fig. 9 *G*, lane *3*) E-cadherin than stock (Fig. 9 *G*, lane *1*) or pp60$^{c\text{-}src+}$-expressing P19 cells (83% of the stock level; Fig. 9 *G*, lane *2*). At this short time after synthesis, an E-cadherin precursor form (pE, 145 kD) predominates, but some of the lower M_r mature E-cadherin can be seen, particularly in the pp60$^{v\text{-}src}$ lane of this exposure (Fig. 9 *G*, lane *3*).

The stability of newly synthesized E-cadherin was determined in a pulse-chase experiment. The half-times for loss of ^{35}S-methionine-labeled E-cadherin in stock, pp60$^{c\text{-}src+}$-expressing, and pp60$^{v\text{-}src}$-expressing P19 cells were found to be 5.6, 3.8, and 3.9 h, respectively. Thus, the higher level of E-cadherin in these pp60$^{v\text{-}src}$-expressing P19 cells can be accounted for by increased synthesis. The lower level of E-cadherin in these pp60$^{c\text{-}src+}$-expressing P19 cells correlates with the faster degradation rate.

The higher level of cell surface E-cadherin in pp60$^{v\text{-}src}$-expressing P19 cells correlates with the tighter cell packing in monolayer cultures of pp60$^{v\text{-}src}$-expressing P19 cells (Fig. 3 *C*). Likewise, lower cell surface levels of E-cadherin in pp60$^{c\text{-}src+}$-expressing P19 cells correlates with less tight cell packing in monolayer cultures of pp60$^{c\text{-}src+}$-expressing cells (Fig. 3 *B*). However, pp60$^{c\text{-}src+}$- and pp60$^{v\text{-}src}$-expressing P19 cells do not have the low level of E-cadherin characteristic of RA-treated P19 cells (Fig. 9 *A*, lane *3*).

Cell surface E-cadherin of aggregated P19 cells is decreased after RA treatment of stock, pp60$^{v\text{-}src}$-expressing, and pp60$^{c\text{-}src+}$-expressing P19 cells (Fig. 9 *D*). However, the level of cell surface E-cadherin in RA-treated aggregates of pp60$^{v\text{-}src}$-expressing P19 cells is greater than in RA-treated aggregates of stock P19 cells (1.5-fold greater; Fig. 9 *D*, lanes *2* and *6*). Thus, we could not correlate decreased cell-cell adhesion observed in pp60$^{v\text{-}src}$-expressing P19 cell aggregates with a decrease in the level of cell surface E-cadherin.

Discussion

Cell-cell contact-dependent signals are an important but mostly unexplored aspect of vertebrate neurogenesis. Our results provide new insights into understanding neurogenesis in the P19 embryonal carcinoma system and suggest that this in vitro system may be useful for the study of cell-cell signals involved in neurogenesis. First, we have found that there is transient expression of an epithelial phenotype by cells in RA-treated aggregates. Second, we have found that while pp60$^{v\text{-}src}$ inhibits neuronal differentiation it does not inhibit epithelial differentiation. Third, our results raise the possibility that PTKs may modulate cell fate during RA-induced differentiation by regulating calcium-dependent cell-cell adhesion. We discuss each of these topics below.

Cell Fates of Retinoic Acid-treated P19 Cells

Differentiating P19 cells have characteristics in common with multipotent cells of the early embryo. The inner cell mass of the mouse embryo does not express significant numbers of intermediate filaments, as determined by EM (26). The calcium-dependent cell-cell adhesion molecule of the inner cell mass and its two earliest derivatives (primitive ectoderm and endoderm) is E-cadherin (66). Both of these derivatives express keratin filaments and desmosomes, although the levels of these two structures are much lower in primitive ectoderm (27). Mesodermal cells and neural cells are derived from the primitive ectoderm by successive phases of recruitment of cells from the ectoderm. When ectodermal cells commit to the mesodermal and neural lineages they lose expression of keratin filaments (27).

Undifferentiated P19 cells have previously been shown to express some cell surface and intracellular markers that are similar to those of primitive neuroectodermal cells (35). However, as judged by their pluripotency (58), E-cadherin expression (Table I), and low level of intermediate filaments, undifferentiated P19 cells also resemble cells of the inner cell mass. Furthermore, P19 cells exposed to RA in the absence

Table I. Summary of Effects of pp60^{src} on the Retinoic Acid-induced Differentiation of P19-O1A1 Cells

	ECAD	NF	Keratin
Undifferentiated			
stock	+++	−	−
c-src	++	−	−
v-src	++++	−	−
Aggregated			
stock	+		+
c-src	+		+
v-src	++		+
Differentiated			
stock		+	−
c-src		+	+
v-src		−	+

Undifferentiated: non-RA-treated monolayer culture. Aggregated: 2-d RA-treated floating aggregates. Differentiated: cells treated for neuronal differentiation and assayed 11 d after exposure to RA. c-src and v-src: pp60$^{c\text{-}src+}$- and pp60$^{v\text{-}src}$-expressing P19-O1A1 cells, respectively. ECAD, E-cadherin; NF, neurofilament; Keratin, TROMA-1-reactive keratin.

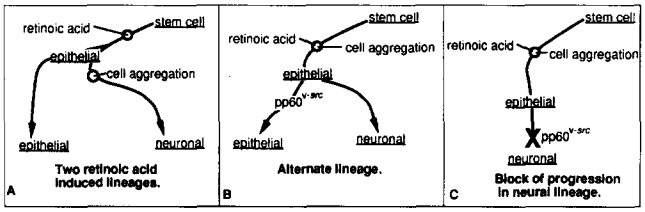

Figure 10. (*A*) The two putative cell-cell contact-dependent lineages of retinoic acid-induced P19-OlA1 cells. (*B* and *C*) Two means by which pp60$^{v\text{-}src}$ might alter cell fate during retinoic acid-induced differentiation of P19-OlA1 cells.

of close cell-cell contact can differentiate into epithelial cells (Fig. 10 *A*), as do cells of the inner cell mass. These considerations, together with the fact that pp60$^{v\text{-}src}$-expressing P19 cells that were treated for neuronal differentiation were found to have undergone epithelial differentiation, prompted us to test if stock P19 cells might transiently express an epithelial phenotype when induced for neuronal differentiation.

We have found that stock P19 cells exposed to RA as floating aggregates are induced to express keratin (Table I). Also, some desmoplakins become resistant to solubilization with nonionic detergent, a property which correlates with the appearance of a punctate staining pattern located at regions of cell-cell contact, consistent with formation of desmosomes. However, levels of TROMA-1-reactive keratin in RA-treated P19 cells are lower than keratin levels in F9 embryonal carcinoma cells. Thus, while RA-induced F9 cell differentiation favors endodermal phenotypes (64), the lower levels of desmosomes and keratin expression in RA-treated and aggregated P19 cells suggest that they may transiently have a primitive ectodermal phenotype. We are further characterizing the epithelial phenotype of RA-treated and aggregated P19 cells in order to test the hypothesis that the behavior of these cells is analogous to the in vivo progression of inner cell mass through primitive ectoderm to the neural lineage.

It has been reported that TROMA-1 antibody does not detect keratin filaments in mouse primitive ectoderm in vivo (30). TROMA-1 has been proposed as a probe specific for Endo-A keratin in endoderm and trophectoderm of the early embryo (30). While some P19 cells exposed to RA in monolayer culture (48, 50) or exposed to DMSO as aggregates (61) undergo endodermal differentiation, it seems unlikely that the transient epithelial cell type of RA-treated P19 cell aggregates is endoderm or trophectoderm since these cells are not on the neural lineage. It seems more likely to us that the transient epithelial phenotype of RA-treated and aggregated stock P19 cells is ectodermal and that the Endo-A is either inappropriately expressed in this in vitro system or that Endo-A is expressed at a low level of ectoderm in vivo that escaped detection (30). As for ectoderm in vivo, terminal neural differentiation of stock P19 cells results in loss of keratin expression and results in neurofilament expression (Table I). We conclude that P19 cells transiently assume an epithelial phenotype before neural differentiation.

The Alteration in P19 Cell Fate Mediated by pp60^{src}

It was previously shown that expression of pp60$^{v\text{-}src}$ does not block epithelial (endodermal) differentiation of F9 cells, but does block RA-induced neuronal and dimethylsulfoxide-induced muscle differentiation of P19 cells (5). Boulter and Wagner suggested that expression of pp60$^{v\text{-}src}$ might not interfere with the earliest events of mouse embryogenesis, only later events such as neural differentiation. Our results are in agreement with this idea and further define the point in P19 cell development at which expression of pp60$^{v\text{-}src}$ becomes effective in blocking further differentiation events. Expression of pp60$^{v\text{-}src}$ or pp60$^{c\text{-}src+}$ in undifferentiated P19 cells inhibits their capacity for neuronal differentiation. However, pp60$^{v\text{-}src}$– and pp60$^{c\text{-}src+}$-expressing P19 cells retain the capacity to differentiate into epithelial cells. Some of the nonneural cells in these cultures at later times after treatment for neuronal differentiation may be myofibroblastic or myoepithelial cells (59), although the proliferation of these cells is greatly inhibited by growth of RA-treated stock P19 cells in serum-free medium.

Two possibilities exist to account for the generation of nonneuronal cells when pp60$^{c\text{-}src+}$– or pp60$^{v\text{-}src}$–expressing P19 cells are treated for neuronal differentiation (Fig. 10). One possibility is that they result from an alternate differentiation pathway separate from the neural lineage (Fig. 10 *B*). Alternatively, we have not ruled out the possibility that these RA-induced, nonneuronal cells might be committed to the neural lineage but blocked from progressing to a mature neuronal phenotype (Fig. 10 *C*). Analysis of expression of additional marker proteins may clarify this question. For example, a newly identified intermediate filament subtype (nestin) has been found in neuroepithelial cells (34). It will be of interest to determine if neurofilament-negative P19 cells in RA-treated cultures express nestin filaments.

While pp60$^{v\text{-}src}$ is a nonphysiological probe of P19 cell differentiation, it is of interest that pp60$^{c\text{-}src}$ over-expression at least partially mimics the action of pp60$^{v\text{-}src}$, consistent with the idea that regulated tyrosine phosphorylation may be physiologically relevant in vertebrate neurogenesis. We conclude that some cells of pp60$^{c\text{-}src+}$-expressing P19 sublines and most cells of pp60$^{v\text{-}src}$-expressing P19 sublines have an altered fate under conditions that give neuronal differentiation of stock P19 cells. It remains to be determined if this modulation of P19 cell fate is due to exit from the neural lineage or blocked progression within the neural lineage.

Cell-Cell Contact, Tyrosine Phosphorylation, and Choice of Cell Fate

Our results suggest that calcium-dependent cell-cell adhesion is required during RA-induced neurogenesis in the P19 system. The role of cell-cell interactions in neural induction has been investigated in both invertebrate and vertebrate systems. In *Xenopus*, results indicative of the spread of a signal laterally within the ectoderm have been described (60). Cell disaggregation and reaggregation experiments with *Xenopus* suggest a role for cell-cell contacts in ectoderm for neural commitment (22). Recent experiments suggest that cadherins can influence the recruitment of ectodermal cells to the neural lineage in *Xenopus* (15). The P19 system may be useful for identification of a cadherin-dependent signal involved in neurogenesis.

While many receptor PTKs have been shown to be activated by diffusible growth factors, PTKs may also be regulated in a cell-cell contact-dependent manner (4). Transmembrane PTKs have been identified that are involved in

neuronal differentiation (4) and survival (29, 31). A *Drosophila* PTK-linked receptor that is activated by the *Elp* mutation allows differentiation of epithelial cells of the eye imaginal disk to yield pigment cells and bristles and inhibits differentiation of sensory neurons and ommatidia of the eye (3). However, in the same system, the *sevenless* PTK is required for the neuronal differentiation of R7 cells (4). Similarly, in transfection experiments, EGF receptor has recently been shown to promote neuronal differentiation of P19 cells (14). Thus, various PTKs may have different effects in multipotential ectodermal precursor cells and committed neuroepithelial cells. The ability of pp60^{src} to weaken cell-cell contacts in early epithelial precursor cells might indirectly interfere with later neuralizing cell fate decisions that normally depend on the controlled cell-cell contact-dependent activation of receptor-linked PTKs.

The pp60$^{v\text{-}src}$– and pp60$^{c\text{-}src+}$–expressing P19 cells have decreased cell-cell contact in RA-treated aggregates. Embryonic stem cells that express pp60$^{v\text{-}src}$ have also been shown to aggregate poorly (6). We are now testing the hypothesis that decreased cell-cell contact and cell-cell communication is involved in the decreased capacity for neuronal differentiation. Specific adhesion proteins like E-cadherin are potential targets for pp60$^{c\text{-}src}$ in P19 cells, but the ability of pp60$^{v\text{-}src}$ and pp60$^{c\text{-}src+}$ to decrease cell-cell and cell-substrate adhesion in many different cell types suggests that a common element such as actin filament depolymerization may be involved. It also seems likely that pp60$^{v\text{-}src}$ has additional actions in pp60$^{v\text{-}src}$–expressing P19 cells independent of the decreased cell-cell contact at the aggregation stage, such as direct inhibition of gap junction communication (18, 65) or NCAM function (7).

Our results with P19 cells suggest that pp60$^{c\text{-}src}$ expression and activity must be kept low in ectodermal precursor cells in order for close cell-cell contact and neurogenesis to occur. RA may make P19 cells competent for neuronal differentiation by increasing expression of keratin and other proteins which are needed to provide the tight cell-cell contact required for a neuralizing cell-cell signal. After commitment, high levels of pp60$^{c\text{-}src}$ may be a consequence of neural commitment and be involved in migration (7), process elongation (2), and secretion (52). However, such proposed roles for *src* may be shared by other src-family members such as *fyn* and *yes*, since mice that do not express pp60$^{c\text{-}src}$ show no gross neuroanatomical defects in the central or peripheral nervous systems (63, J. Deitch and J. S. Brugge, unpublished).

We thank Joel Levine for cells and for helpful discussions; Dusty Miller for cells and plasmids; and Virginia Lee, Barbara Knowles, Rolf Kemler, and Manijeh Pasdar for antibodies. We thank Mike Demarco for preparing 327 anti-src mAb; Sarah Parsons for EC10 antibody; Shiela Thomas for the pLNSL7v-*src* and pLNCXc-*src* plasmids; and Arnold Levine for F9 cells. We thank Jim Marrs, R. William Mays, and Debra Wollner for critical reading of this manuscript.

J. W. Schmidt was funded as a Burroughs Wellcome Fellow of the Life Sciences Research Foundation. This work was also supported by grants from the National Institutes of Health to W. J. Nelson (GM35527) and J. S. Brugge (CA47572). W. J. Nelson is an established investigator of the American Heart Association.

Received for publication 16 August 1991 and in revised form 26 October 1991.

References

1. Adamson, E. D., H. Baribault, and R. Kemler. 1990. Altered uvomorulin expression in a noncompacting mutant cell line of F9 embryonal carcinoma cells. *Dev. Biol.* 138:338–347.
2. Alema, S., P. Casalbore, E. Agostini, and F. Tato. 1985. Differentiation of PC12 pheochromocytoma cells induced by v-*src* oncogene. *Nature (Lond.).* 316:557–559.
3. Baker, N. E., and G. M. Rubin. 1989. Effect on eye development of dominant mutations in *Drosophila* homologue of the EGF receptor. *Nature (Lond.).* 340:150–153.
4. Banerjee, U., and S. L. Zipursky. 1990. The role of cell-cell interaction in the development of the *Drosophila* visual system. *Neuron.* 4:177–187.
5. Boulter, C. A., and E. F. Wagner. 1988. The effects of v-*src* expression on the differentiation of embryonal carcinoma cells. *Oncogene.* 2:207–214.
6. Boulter, C. A., A. Aguzzi, R. L. Williams, E. F. Wagner, M. J. Evans, and R. Beddington. 1991. Expression of v-*src* induces aberant development and twinning in chimeric mice. *Development (Camb.).* 111:357–366.
7. Brackenbury, R., E. Greenberg, and G. M. Edelman. 1984. Phenotypic changes and loss of N-CAM-mediated adhesion in transformed embryonic chicken retinal cells. *J. Cell Biol.* 99:1944–1955.
8. Brugge, J. S., P. C. Cotton, A. E. Queral, J. N. Barrett, D. Nonner, and R. W. Keane. 1985. Neurons express high levels of a structurally modified, activated form of pp60$^{c\text{-}src}$. *Nature (Lond.).* 316:554–557.
9. Campione-Piccardo, J., J.-J. Sun, J. Craig, and M. W. McBurney. 1985. Cell-cell interaction can influence drug-induced differentiation of murine embryonal carcinoma cells. *Dev. Biol.* 109:25–31.
10. Cepco, C. L. 1989. Immortalization of neural cells via retrovirus-mediated oncogene transduction. *Annu. Rev. Neurosci.* 12:47–66.
11. Coussens, P. M., J. A. Cooper, T. Hunter, and D. Shalloway. 1985. Restriction of the in vitro and in vivo tyrosine protein kinase activities of pp60$^{c\text{-}src}$ relative to pp60$^{v\text{-}src}$. *Mol. Cell. Biol.* 5:2753–2763.
12. Davis, L. G., M. D. Dibnar, and J. F. Battey. 1986. Calcium phosphate transfection of nonadherant and adherant cells with purified plasmids. *In* Basic Methods in Molecular Biology. Elsevier Science Publishing Co., New York. 286–289.
13. DeLorb, W. J., P. A. Luciw, H. M. Goodman, H. E. Varmus, and J. M. Bishop. 1980. Molecular cloning and characterization of avian sarcoma virus circular DNA molecules. *J. Virol.* 36:50–61.
14. den Hertog, J., S. W. de Laat, J. Schlessinger, and W. Kruijer. 1991. Neuronal differentiation in response to epidermal growth factor of transfected murine P19 embryonal carcinoma cells expressing human epidermal growth factor receptors. *Cell Growth Diff.* 2:155–164.
15. Detrick, R. J., D. Dickey, and C. R. Kintner. 1990. Effects of N-cadherin misexpression on morphogenesis in *Xenopus* Embryos. *Neuron.* 4:493–506.
16. Edwards, M. K. S., and M. W. McBurney. 1983. The concentration of retinoic acid determines the differentiation cell types formed by a teratocarcinoma cell line. *Dev. Biol.* 98:187–191.
17. Falconer, M. M., U. Vielkind, and D. L. Brown. 1989. Association of acetylated microtubules, vimentin intermediate filaments, and MAP2 during early neural differentiation in EC cell culture. *Biochem. Cell. Biol.* 67:537–544.
18. Filson, A. J., R. Azarnia, E. C. Beyer, W. R. Lowenstein, and J. S. Brugge. 1990. Tyrosine phosphorylation of gap junction protein correlates with inhibition of cell-to-cell communication. *Cell Growth Diff.* 1:661–668.
19. Glenney, J. R., L. Zokas, and M. P. Kamps. 1988. Monoclonal antibodies to phosphotyrosine. *J. Immunol. Methods.* 109:277–285.
20. Golden, A., and J. S. Brugge. 1989. Thrombin treatment induces rapid changes in tyrosine phosphorylation in platelets. *Proc. Natl. Acad. Sci. USA.* 86:901–905.
21. Gorman, C. M., P. W. J. Rigby, and D. P. Lane. 1985. Negative regulation of viral enhancers in undifferentiated embryonic stem cells. *Cell.* 42:519–526.
22. Grunz, H., and L. Tacke. 1989. Neural differentiation of *Xenopus* laevis takes place after disaggregation and delayed reaggregation without inducer. *Cell Diff. Dev.* 28:211–218.
23. Haltmeier, H., and H. Rohrer. 1990. Distinct and different effects of the oncogenes v-*myc* and v-*src* on avian sympathetic neurons: retroviral transfer of v-*myc* stimulates neuronal proliferation whereas v-*src* transfer enhances differentiation. *J. Cell Biol.* 110:2087–2098.
24. Howe, W. E., F. G. Klier, and R. G. Oshima. 1986. Murine endodermal cytokeratins Endo A and Endo B are localized to the same intermediate filament. *J. Histochem. Cytochem.* 34:785–793.
25. Iba, H., T. Takeya, F. R. Cross, T. Hanafusa, and H. Hanafusa. 1984. Rous sarcoma virus variants that carry the cellular *src* gene instead of the viral *src* gene cannot transform chicken embryo fibroblasts. *Proc. Natl. Acad. Sci. USA.* 81:4424–4428.
26. Jackson, B. W., C. Grund, E. Schmid, K. Burki, W. W. Franke, and K. Illmensee. 1980. Formation of cytoskeletal elements during mouse embryogenesis. *Differentiation.* 17:161–179.
27. Jackson, B. W., C. Grund, S. Winter, W. W. Franke, and K. Illmensee.

1981. Formation of cytoskeletal elements during mouse embryogenesis II. Epithelial differentiation and intermediate-sized filaments in early postimplantation embryos. *Differentiation.* 20:302–216.
28. Jones-Villenuve, E. M. V., M. W. McBurney, K. A. Rogers, and V. I. Kalnins. 1982. Retinoic acid induces embryonal carcinoma cells to differentiate into neurons and glial cells. *J. Cell Biol.* 94:253–262.
29. Kaplan, D. R., B. L. Hempstead, D. Martin-Zanca, M. V. Chao, and L. F. Parada. 1991. The *trk* proto-oncogene product: a signal transducing receptor for nerve growth factor. *Science (Wash. DC).* 252:554–558.
30. Kemler, R., P. Brulet, M. T. Schenebelin, J. Gaillard, and F. Jacob. 1981. Reactivity of monoclonal antibodies against intermediate filament proteins during embryonic development. *J. Embryol. Exp. Morphol.* 64: 45–60.
31. Klein, R., S. Jing, V. Nanduri, E. O'Rourke, and M. Barbacid. 1991. The *trk* proto-oncogene encodes a receptor for nerve growth factor. *Cell.* 65:189–197.
32. Kurki, P., A. Laasonen, E. M. Tan, and E. Lehtonen. 1989. Cell proliferation and expression of cytokeratin filaments in F9 embryonal carcinoma cells. *Development (Camb.).* 106:635–640.
33. Lee, V. M.-Y., M. J. Carden, W. W. Schlaepfer, and J. Q. Trojanowski. 1987. Monoclonal antibodies distinguish several differentially phosphorylated states of the two largest rat neurofilament subunits (NF-H and NF-M) and demonstrate their existence in the normal nervous system of adult rats. *J. Neurosci.* 7:3474–3488.
34. Lendahl, U., L. B. Zimmerman, and R. G. D. Mckay. 1990. CNS stem cells express a new class of intermediate filament protein. *Cell.* 60: 585–595.
35. Levine, J. M., and P. Flynn. 1986. Cell surface changes accompanying the neural differentiation of an embryonal carcinoma cell line. *J. Neurosci.* 6:3374–3384.
36. Levy, J. B., and J. S. Brugge. 1989. Biological and biochemical properties of the c-src$^+$ gene product overexpressed in chicken embryo fibroblasts. *Mol. Cell. Biol.* 9:3332–3341.
37. Levy, J. B., H. Iba, and H. Hanafusa. 1986. Activation of the transforming potential of pp60$^{c\text{-}src}$ by a single amino acid change. *Proc. Natl. Acad. Sci. USA.* 83:4228–4232.
38. Levy, J. B., T. Dorai, L.-H. Wang, and J. S. Brugge. 1987. The structurally distinct form of pp60$^{c\text{-}src}$ detected in neuronal cells is encoded by a unique c-*src* mRNA. *Mol. Cell. Biol.* 7:4142–4145.
39. Lipsich, L. A., A. J. Lewis, and J. S. Brugge. 1983. Isolation of monoclonal antibodies that recognize the transforming protein of avian sarcoma viruses. *J. Virol.* 48:352–360.
40. Littlefield, J. W. 1989. Stepwise aggregation, compaction, and differentiation of uncompacted F9 cells. *Dev. Gene.* 10:402–410.
41. Lynch, S. A., J. S. Brugge, and J. M. Levine. 1986. Induction of altered c-*src* product during neural differentiation of embryonal carcinoma cells. *Science (Wash DC).* 234:873–876.
42. Mann, R., R. C. Mulligan, and D. B. Baltimore. 1983. Construction of a retrovirus packaging mutant and its use to produce helper-free defective retrovirus. *Cell.* 33:153–159.
43. Martinez, R., B. Mathey-Prevot, A. Bernards, and D. Baltimore. 1987. Neuronal pp60$^{c\text{-}src}$ contains a six-amino acid insert relative to its nonneuronal counterpart. *Science (Wash. DC).* 237:411–415.
44. McBurney, M. W., K. R. Reuhl, A. I. Ally, S. Nasipuri, J. C. Bell, and J. Craig. 1988. Differentiation and maturation of embryonal carcinoma-derived neurons in cell culture. *J. Neurosci.* 8:1063–1073.
45. Melton, D. A. 1991. Pattern formation during animal development. *Science (Wash. DC).* 252:234–241.
46. Miller, A. D., and G. J. Rosman. 1989. Improved retroviral vectors for gene transfer and expression. *Biotechniques.* 7:980–990.
47. Moll, R., P. Cowin, H.-P. Kaprell, and W. W. Franke. 1986. Desmosomal proteins: new markers for identification and classification of tumors. *Lab. Invest.* 54:4–25.
48. Mummery, C. L., C. E. van den Brink, and S. W. de Laat. 1987. Commitment to differentiation induced by retinoic acid in P19 embryonal carcinoma cells is cell cycle dependent. *Dev. Biol.* 121:10–19.
49. Mummery, C. L., A. Feyen, E. Freund, and S. Shen. 1990. Characteristics of embryonic stem cell differentiation: a comparison with two embryonal carcinoma cell lines. *Cell Diff. Dev.* 30:195–206.
50. Mummery, C. L., W. Kruijer, E. Feijen, E. Freund, I. Koornneef, and V. D. E.-V. Raaij. 1990. Expression of transforming growth factor β2 during the differentiation of murine embryonal carcinoma and embryonic stem cells. *Dev. Biol.* 137:161–170.
51. Nelson, W. J., and P. Veshnock. 1986. Dynamics of membrane-skeleton (fodrin) organization during development of polarity in Madin-Darby canine kidney epithelial cells. *J. Cell Biol.* 103:1751–1765.
52. Oddie, K. M., J. C. Balserak, D. M. Payne, C. E. Creutz, and S. J. Parsons. 1989. Modulation of pp60$^{c\text{-}src}$ tyrosine kinase activity during secretion in stimulated bovine chromaffin cells. *J. Neurosci. Res.* 24: 38–48.
53. Ozawa, M., H. Baribault, and R. Kemler. 1989. The cytoplasmic domain of the cell adhesion molecule uvomorulin associates with three independent proteins structurally related in different species. *EMBO (Eur. Mol. Biol. Organ.) J.* 8:1711–1717.
54. Parsons, S. J., D. J. McCarley, V. W. Raymond, and J. T. Parsons. 1986. Localization of conserved and nonconserved epitopes within the Rous sarcoma virus-encoded *src* protein. *J. Virol.* 59:755–758.
55. Pasdar, M., and W. J. Nelson. 1988. Kinetics of desmosome assembly in Madin-Darby canine kidney epithelial cells: temporal and spatial regulation of desmoplakin organization and stabilization upon cell-cell contact. I. Biochemical analysis. *J. Cell Biol.* 106:677–686.
56. Pawson, T., and A. Bernstein. 1990. Receptor tyrosine kinases: genetic evidence for their role in *Drosophila* and mouse development. *Trends Genet.* 6:350–356.
57. Rodriguez-Boulan, E., and W. J. Nelson. 1989. Morphogenesis of the polarized epithelial cell phenotype. *Science (Wash. DC).* 245:718–725.
58. Rossant, J., and M. W. McBurney. 1982. The developmental potential of a euploid male teratocarcinoma cell line after blastocyst injection. *J. Embryol. Exp. Morphol.* 70:99–112.
59. Rudnicki, M. A., N. M. Sawtell, K. R. Reul, R. Berg, J. C. Craig, K. Jardine, J. L. Lessard, and M. W. McBurney. 1990. Smooth muscle actin expression during P19 embryonal carcinoma differentiation in cell culture. *J. Cell. Physiol.* 142:89–98.
60. Ruiz i Altaba, A. 1990. Neural expression of the *Xenopus* homeobox gene Xhox3: evidence for a patterning signal that spreads through the ectoderm. *Development (Camb.).* 108:595–604.
61. Smith, S. C., K. R. Reuhl, J. Craig, and M. W. McBurney. 1987. The role of aggregation in embryonal carcinoma cell differentiation. *J. Cell. Physiol.* 131:74–84.
62. Solter, D., and B. B. Knowles. 1978. Monoclonal antibody defining a stage-specific mouse embryonic antigen (SSEA-1). *Proc. Natl. Acad. Sci. USA.* 75:5565–5569.
63. Soriano, P., C. Montgomery, R. Geske, and A. Bradley. 1991. Targeted disruption of the c-src proto-oncogene leads to osteopetrosis in mice. *Cell.* 64:693–702.
64. Strickland, S., K. K. Smith, and K. R. Marotti. 1980. Hormonal induction of differentiation in teratocarcinoma stem cells: generation of parietal endoderm by retinoic acid and dibutyryl cAMP. *Cell.* 21:347–355.
65. Swenson, K. I., H. Piwnica-Worms, H. McNamee, and D. L. Paul. 1990. Tyrosine phosphorylation of the gap junction protein connexin43 is required for the pp60$^{v\text{-}src}$-induced inhibition of communication. *Cell Reg.* 1:989–1002.
66. Takeichi, M. 1988. The cadherins: cell-cell adhesion molecules controlling animal morphogenesis. *Development (Camb.).* 102:639–655.
67. Vestweber, D., and R. Kemler. 1984. Rabbit antiserum against a purified surface glycoprotein decompacts mouse preimplantation embryos and reacts with specific adult tissues. *Exp. Cell Res.* 152:169–178.
68. Volberg, T., B. Geiger, R. Dror, and Y. Zick. 1991. Modulation of intercellular adherens-type junctions and tyrosine phosphorylation of their components in RSV-transformed cultured chick lens cells. *Cell Reg.* 2:105–120.
69. Warren, S. L., and W. J. Nelson. 1987. Nonmitogenic morphoregulatory action of pp60$^{v\text{-}src}$ on multicellular epithelial structures. *Mol. Cell. Biol.* 7:1326–1337.